



University of  
Massachusetts  
Amherst

## Evaluating a Novel Photochemical Tool for Labeling and Tracking Live, Endogenous Calcium-Permeable AMPARs

Item Type	Thesis (Open Access)
Authors	Combs-Bachmann, Rosamund Elizabeth
DOI	<a href="https://doi.org/10.7275/8748533">10.7275/8748533</a>
Download date	2026-03-07 03:21:06
Link to Item	<a href="https://hdl.handle.net/20.500.14394/33347">https://hdl.handle.net/20.500.14394/33347</a>

**EVALUATING A NOVEL PHOTOCHEMICAL TOOL  
FOR LABELING AND TRACKING LIVE,  
ENDOGENOUS CALCIUM-PERMEABLE  
AMPARS**

A Thesis Presented

By

ROSAMUND ELIZABETH COMBS-BACHMANN

Submitted to the Graduate School of the  
University of Massachusetts Amherst in partial fulfillment  
of the requirements for the degree of

MASTER OF SCIENCE

May 2016

Neuroscience and Behavior Program

© Copyright by Rosamund Combs-Bachmann 2016  
All Rights Reserved

**EVALUATING A NOVEL PHOTOCHEMICAL TOOL  
FOR LABELING AND TRACKING LIVE,  
ENDOGENOUS CALCIUM-PERMEABLE  
AMPARS**

A Thesis Presented

By

ROSAMUND ELIZABETH COMBS-BACHMANN

Approved as to style and content by:

---

James J. Chambers, Chair

---

Gerald B. Downes, Member

---

Jerrold S. Meyer, Member

---

Luke Ramage-Healey, Member

---

Betsy Dumont, Director  
Interdisciplinary Programs for the Life Science

ABSTRACT

**EVALUATING A NOVEL PHOTOCHEMICAL TOOL FOR LABELING AND  
TRACKING LIVE, ENDOGENOUS CALCIUM-PERMEABLE AMPARS**

MAY 2016

ROSAMUND ELIZABETH COMBS-BACHMANN, B.S., GUILFORD COLLEGE

M.S., UNIVERSITY OF MASSACHUSETTS AMHERST

Directed by: Professor James J. Chambers

The purpose of this research is to advance development of a photochemical tool designed to probe the role of ionotropic glutamate receptor signaling in neurodegenerative processes, and to delve more deeply into the biological processes underlying the role of these receptors in signaling and memory formation. This ligand-targeted nanoprobe was designed and developed in our lab to label endogenous calcium-permeable AMPARs (CP-AMPARs) in live cells with minimal disruption to native receptor activity. Nanoprobe is designed to use naphthyl acetyl spermine (NASPM) as a photocleavable ligand to target and covalently label native CP-AMPARs with a non-perturbing, fluorescent marker that then allows observation of these receptors using standard epifluorescence microscopy. My contribution to this work, outlined in the aims below, is the characterization of nanoprobe using electrophysiology and fluorescent imaging to evaluate its effectiveness as an endogenous CP-AMPAR label on live neurons.

**Aim 1:** To use whole cell patch clamp electrophysiology to test the labeling of CP-AMPARs with nanoprobe by recording changes in glutamate-evoked current through heterologously expressed GluA1-L497Y homomultimers during, pre- and post-nanoprobe labeling.

**Aim 2:** To use fluorescent imaging to evaluate nanoprobe labeling of glutamate receptors endogenously expressed in hippocampal neurons by co-labeling nanoprobe-treated neurons with traditional antibodies to AMPAR and synaptic targets.

**Aim 3:** To use nanoprobe to detect endogenously expressed CP-AMPARs on live neurons during the course of neuron development. Live neuronal cultures will be imaged before and after labeling with nanoprobe in young dissociated cultures (DIV 1-2) and in maturing cultures (DIV 14-17).

**Conclusions:** Whole cell patch clamp electrophysiology results provide evidence that nanoprobe will label CP-AMPARs in a minimally-perturbing fashion that allows the receptors to resume normal activity after photolytic-release of ligand as designed. Fixed cell imaging of CP-AMPAR nanoprobe labeling was largely ineffective, and live cell imaging was not conclusive, but provided supporting evidence that nanoprobe targets and labels NASPM-sensitive endogenous glutamate receptors on live dissociated hippocampal neurons.

# TABLE OF CONTENTS

	Page
ABSTRACT .....	iv
LIST OF FIGURES.....	viii
CHAPTER	
1. INTRODUCTION .....	1
2. BACKGROUND AND SIGNIFICANCE .....	2
Ionotropic glutamate receptor architecture.....	2
Role of CP-AMPARs in synaptic development and neuronal plasticity.....	4
CP-AMPAR expression levels during development.....	8
Role of CP-AMPARs in injury and disease.....	9
Role of CP-AMPARs in drug addiction.....	14
Use of endogenous polyamines and neurotoxins to target CP-AMPARs ....	15
Nanoprobe for labeling CP-AMPARs .....	20
3. RESEARCH DESIGN AND METHODS.....	23
Aim 1: Whole cell patch clamp electrophysiology .....	23
Aim 2: Imaging co-labeled endogenous receptors.....	28
Aim 3: Imaging and tracking nanoprobe-labeled receptors on live neurons .....	31

Dose-dependent labeling of live neurons with nanoprobe .....	32
Co-incubation with competitor molecules .....	33
Tracking movements of nanoprobe-labeled receptors in young and maturing cultures .....	34
Co-incubation with mitochondrial label.....	35
4. EXPECTED RESULTS.....	36
Aim 1: Whole cell patch clamp electrophysiology .....	36
Aim 2: Imaging co-labeled endogenous receptors.....	37
Aim 3: Imaging and tracking nanoprobe-labeled receptors on live neurons .....	39
5. RESULTS.....	41
Aim 1: Whole cell patch clamp electrophysiology .....	41
Aim 2: Imaging co-labeled endogenous receptors.....	46
Aim 3: Imaging and tracking nanoprobe-labeled receptors on live neurons .....	64
Dose-dependent labeling of live neurons with nanoprobe .....	65
Nanoprobe labeling of live neurons is prevented by co-incubation with competitor molecules.....	66
Tracked movements of nanoprobe-labeled receptors: DIV 14-17 .....	71
Tracked movements of nanoprobe-labeled receptors: DIV 1-2.....	76
REFERENCES.....	84

## LIST OF FIGURES

Figure	Page
1. Iontropic glutamate receptor (iGluR) architecture.....	4
2. Nanoprobe design and labeling of active CP-AMPARs. ....	21
3. Photocleaving ligand after nanoprobe labeling leaves probe fluorophore bound to unperturbed CP-AMPAR.....	22
4. Nanoprobe application during whole cell patch clamp electrophysiology of HEK293T cells expressing CP-AMPARs.....	24
5. CP-AMPAR glutamate response recorded with whole cell patch clamp electrophysiology.....	26
6. Nanoprobe block of CP-AMPAR glutamate response, and release of block via photolysis, recorded with whole cell patch clamp electrophysiology.....	27
7. Whole cell patch clamp data from HEK293T cells expressing GluA1-L497Y homomeric receptors.....	45
8. Punctate staining of DIV 14 dissociated hippocampal culture treated with 100 $\mu$ M nanoprobe.....	48
9. Punctate patterns of fluorescence in DIV 14 dissociated hippocampal culture treated with 100 $\mu$ M nanoprobe, using neurons pictured in Figure 8. ....	51
10. DIV 24 dissociated hippocampal culture co-labeled with nanoprobe and anti-GluA1 shows little to no colocalization of the two fluorescent labels.....	52
11. Visualizing nanoprobe and anti-GluA1 colocalization.....	54
12. Visualizing nanoprobe and anti-GluA1 colocalization.....	55
13. Co-labeling neurons with pan-AMPAR antibody and nanoprobe does not result in clear probe labeling of receptors.....	56
14. Nanoprobe fluorescent labeling (red) colocalized with anti-synapsin-1 Cell Signaling antibody (green).....	58
15. Nanoprobe fluorescent labeling (red) rarely colocalizes with anti-synapsin-1 Cell Signaling antibody (green).....	60

16. Images of untreated neurons express significant autofluorescence in the red channel.....	60
17. Images of randomly selected regions of coverslips treated with nanoprobe for varying times at varying concentrations failed to reveal any clear probe labeling in punctate patterns above background fluorescence.....	62
18. Coverslips treated for varying times with glutamate and with varying nanoprobe concentrations did not reveal any clear probe labeling in punctate patterns, though increased clustering of objects fluorescing in the red channel was seen.....	62
19. Nanoprobe labels DIV 14–17 neurons in a concentration-dependent manner and can be blocked by competitive antagonists.....	67
20. Movements of nanoprobe-labeled receptors.....	74
21. Local movements of fluorescence into spines.....	76
22. Dynamic tubular vesicles in DIV 1 dissociated hippocampal neurons treated with nanoprobe.....	77
23. Competitive antagonist DNQX blocks nanoprobe labeling of DIV 1-2 neurons.....	77
24. Competitive antagonist NASPM blocks nanoprobe labeling of DIV 1-2 neurons.....	78
25. Dual-labeling of DIV 1 neurons with nanoprobe and a mitochondrial label shows extensive overlap.....	82
26 and 27. Dual-labeling of DIV 1 neurons with nanoprobe and a mitochondrial label shows extensive overlap, and clear delineations where overlap ends.....	83

# CHAPTER 1

## INTRODUCTION

Normal communication in a healthy nervous system requires rapid transmission of information between neurons. This inter-neuronal communication is typically mediated chemically, via release of neurotransmitters into the synaptic cleft. One of the main neurotransmitters involved in this synaptic communication is glutamate, the primary excitatory neurotransmitter found in the central nervous system (CNS). The ionotropic glutamate receptors known as AMPA (2-amino-3-(5-methyl-3-oxo-1,2-oxazol-4-yl)propanoic acid) receptors play a key role both in regulating excitatory signaling between neurons, and in long term potentiation (LTP), a type of synaptic plasticity thought to underlie memory formation. Malfunctions in ionotropic glutamatergic signaling due to alterations in mRNA editing, AMPAR trafficking and localization, or AMPAR channel kinetics can lead to destruction of synaptic spines and even of whole neurons. These destructive processes are implicated in a number of neurodegenerative disorders. While the majority of AMPARs allow only sodium ions to enter the post-synaptic neuron, calcium-permeable AMPA receptors (CP-AMPARs) allow calcium ions to enter as well, and thus have a unique role to play in disease processes and memory formation. CP-AMPARs have been implicated in the motor neuron loss that is the hallmark of the degenerative disease Amyotrophic Lateral Sclerosis (ALS), as well as in neuronal plasticity underlying processes involved in memory formation and extinction, models of drug addiction and epilepsy.

## CHAPTER 2

### BACKGROUND AND SIGNIFICANCE

Glutamate is the primary excitatory neurotransmitter in the CNS (central nervous system), and ionotropic glutamate receptors such as AMPA (amino-3-(5-methyl-3-oxo-1,2-oxazol-4-yl)propanoic acid) receptors, kainate receptors, and NMDA (*N*-methyl-D-aspartic acid) receptors play a key role in regulating excitatory signaling between neurons. Ionotropic glutamatergic signaling is critical to the synaptic plasticity underlying learning and memory, and malfunctions in this signaling can lead to destruction of synaptic spines and of whole neurons. These destructive processes are implicated in a number of neurodegenerative disorders.

#### Ionotropic glutamate receptor architecture

AMPA receptors, NMDA receptors, and kainate receptors, are all ionotropic glutamate receptors that share a number of structural similarities. Each functional receptor is composed of a tetramer of subunits that combine to create a central ligand-gated ion channel. Typically each receptor is composed of at least two different types of subunit per receptor, though AMPA receptors and kainate receptors can form homotetramers as well. There are four AMPA receptor subunits (GluA1-GluA4), five kainate receptor subunits (GluK1-GluK5), and 3 NMDA subunits (GluN1, GluN2 and GluN3). GluN2 and GluN3 subunits each have several subtypes of their own (GluN2A-D, and GluN3A-B). Each subunit has an intracellular carboxy-terminal tail (c-tail), a transmembrane region, and an extracellular region where glutamate and other agonists and antagonists can bind. The extracellular region consists of a ligand-binding domain,

and an amino-terminal domain which is involved in receptor formation, membrane targeting and trafficking, and in the case of NMDARs, regulation of signaling by binding allosteric modulators. The transmembrane region is primarily composed of four helices (M1, M2, M3, and M4) that line the ion channel pore, three of which completely span the membrane and one re-entrant loop that only partially spans the membrane (Traynelis et al., 2010). Figure 1 illustrates these components with a cartoon of two AMPAR subunits in a phospholipid bilayer.

The re-entrant loop of AMPAR subunits and kainate receptor subunits GluK1 and GluK2 contains a variable site (the Q/R site) which determines calcium permeability of the ion channel. When this site contains an uncharged glutamine (Q) for all four subunits, calcium ions can pass through the channel. However this neutral glutamine can be changed to a positively charged arginine through posttranscriptional mRNA editing, as is the case for the large majority of GluA2 subunits (Sobolevsky et al., 2009; Traynelis et al., 2010). This editing event results in functional channels that do not pass calcium.

Typically AMPARs are composed of GluA1, 3, or 4 in combination with GluA2, causing the majority of AMPARs to be calcium-impermeable. When glutamate binds to calcium-impermeable AMPARs (CI-AMPARs) the intrinsic ion channel opens to allow monovalent cations, primarily sodium ions, to flow into the post-synaptic neuron and locally depolarize the membrane. However, a subset of AMPARs are calcium-permeable, either because they lack the GluA2 subunit or because they include an unedited GluA2 subunit. When glutamate binds these calcium-permeable AMPARs (CP-AMPARs) the intrinsic ion channel opens and allows both sodium and calcium

ions to pass through the channel and into the post-synaptic neuron. The regulation of calcium influx into synapses is critical to regulating activity-dependent synaptic plasticity, and ongoing research is demonstrating that these calcium-permeable AMPARs (CP-AMPARs) have a greater role in synaptic plasticity and neuronal development than was previously thought.

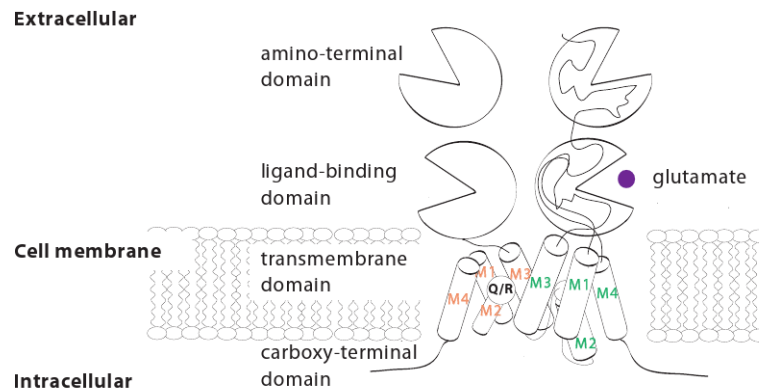


**Figure 1: Ionotropic glutamate receptor (iGluR) architecture.** iGluRs are composed of four subunits that form a transmembrane ion channel. Shown here is a cartoon of two of the four subunits that compose an AMPA receptor. Editing at the Q/R site determines calcium permeability of GluA1-4 and GluK1-2 subunits.

## Role of CP-AMPA receptors in synaptic development and neuronal plasticity

Glutamate receptors are central to many of the mechanisms involved in neuronal adaptation and plasticity. In response to changes in neuronal activity these receptors can be added to, or removed from, synapses, and these activity-dependent modifications are thought to underlie many types of experience-dependent plasticity

including learning and memory formation. Long-term potentiation (LTP) and long-term depression (LTD) are the two most ubiquitous and well-understood forms of this neuronal plasticity. Examples of both have been found at excitatory synapses throughout the brain. These synaptic modifications act to either strengthen the response of the post-synaptic neuron to excitatory signaling at that synapse (LTP), or to weaken the response (LTD). Both depend on calcium influx across the post-synaptic membrane, and both involve a number of synaptic modifications, including insertion (LTP) and removal (LTD) of AMPARs at the synapse (Kessels & Malinow, 2009; Luscher & Malenka, 2012; Malenka & Bear, 2004).

The classic, most widely studied model of activity-dependent modification is NMDAR-dependent LTP, which requires surface-expressed NMDA receptors to provide the channels through which calcium can influx into the neuron and trigger downstream plasticity (Bliss & Collingridge, 1993; Huganir & Nicoll, 2013; Malenka & Bear, 2004). However CP-AMPARs are also capable of providing the necessary route for calcium to enter neurons and trigger synaptic plasticity. Increasingly, researchers are finding examples of CP-AMPARs mediating activity-dependent synaptic modifications such as LTP and LTD, frequently in conjunction with signaling from other receptor types, such as group I metabotropic glutamate receptors (mGluRs) (Camire & Topolnik, 2014; Hainmuller et al., 2014; Kullmann & Lamsa, 2008; Le Duigou & Kullmann, 2011) or nicotinic acetylcholine receptors (nAChRs) (Griguoli et al., 2013).

Often the described examples of CP-AMPAR-mediated LTP are specifically examples of ‘anti-Hebbian’ LTP, which requires simultaneous pre-synaptic glutamate release and post-synaptic hyperpolarization (Lamsa et al., 2007; Le Duigou & Kullmann,

2011; Le Roux et al., 2013; Oren et al., 2009; Szabo et al., 2012). When the neuronal membrane is depolarized CP-AMPARs are blocked by endogenous intracellular polyamines, while at resting or hyperpolarized potentials the CP-AMPAR intrinsic ion channel is unblocked allowing calcium influx. This decrease of current through the receptors as the membrane is depolarized is described as inward rectification. The term ‘anti-Hebbian’ was coined to differentiate this process from classic ‘Hebbian’ LTP, which is NMDA-dependent and requires pre-synaptic glutamate release and post-synaptic *depolarization*. In Hebbian LTP the post-synaptic depolarization is necessary to repel the positively charged extracellular magnesium ions that typically block the NMDAR intrinsic ion channel at resting membrane potentials (Kullmann & Lamsa, 2007). Interestingly, some evidence suggests that anti-Hebbian LTP is pre-synaptically expressed (Lamsa et al., 2007; Nicholson & Kullmann, 2014), although Le Roux et al. (2013) suggests that at least in the specific case of CA1 parvalbumin interneurons, only post-synaptic LTP is present. There has also been at least one demonstration of apparent Hebbian LTP mediated in part by CP-AMPARS (Hainmuller et al., 2014). In this example the patch pipette solution contained spermine to maintain CP-AMPAR inward rectification, avoiding Hebbian LTP due to lack of intracellular polyamine block during membrane depolarization.

In young (2.5-4 weeks old) rodent models, aspiny GABAergic interneurons are one of the most well-established sites of CP-AMPAR expression and NMDAR-independent LTP (Nissen et al., 2010; Oren et al., 2009; Polepalli et al., 2010; Sambandan et al., 2010; Szabo et al., 2012). One explanation for the prevalence of CP-AMPARs on aspiny neurons is that they may help make LTP and other forms of plasticity synapse-specific

in the absence of dendritic spines. The morphology of dendritic spines provides a physical means of compartmentalizing influxing calcium and downstream molecular components of plasticity, helping to keep synaptic alterations specific to the active synapses where calcium is entering (Bourne & Harris, 2008; Goldberg et al., 2003; Yuste & Denk, 1995). As aspiny neurons lack this morphological means of compartmentalizing calcium and downstream signaling cascades, the question arises as to how they participate in synapse-specific plasticity. There are a number of mechanisms that likely contribute to containment of plasticity-related signaling, including barriers to diffusion of calcium and other small molecules (Soler-Llavina & Sabatini, 2006) and the rapid removal of calcium via the calcium/sodium exchanger (Goldberg et al., 2003). The rapid kinetics of CP-AMPARs provide an additional means of biochemical compartmentalization, restricting calcium to microdomains at the synapse (Angulo et al., 1999; Goldberg et al., 2003; Laezza & Dingledine, 2011).

There is also some evidence to suggest that CP-AMPARs can play a role in NMDAR-dependent LTP, though this finding is controversial. Plant et al. (2006) found evidence that CP-AMPARs are transiently expressed shortly after LTP induction in pyramidal neurons of the hippocampal CA1 region, and are replaced with CI-AMPARs within the first half hour. The authors suggest that these CP-AMPARs help to stabilize LTP at the involved synapses. However, a follow-up study by Adesnik and Nicoll (2007) failed to find evidence of CP-AMPAR expression following LTP induction in these same neurons. Putting this apparent contradiction in a slightly different light, Mattison et al. (2014), found that spines on apical dendrites in CA1 pyramidal neurons appeared to have a population of CP-AMPARs, while spines on basal dendrites did

not. This implies it would be possible to find CP-AMPA absence and involvement at synapses on the same neuron, depending on which dendrites were examined. Finally, Clem and Huganir (2010) found evidence that transient expression of CP-AMPA on a slower time scale helps consolidate fear memories at thalamic inputs to the lateral amygdala. An increase in CP-AMPA expression was detected hours after auditory fear conditioning in mice, and was gone after seven days. Removal of these CP-AMPA one day after conditioning via a reconsolidation update protocol was key to erasing these fear memories. Use of this same protocol on the seventh day following conditioning failed to erase the fear memory.

### **CP-AMPA expression levels during development**

CP-AMPA are expressed at higher levels in developing brains than in adult brains, and a number of animal model studies have linked CP-AMPA expression levels to neuronal development. While AMPA in the adult CNS predominately contain the edited GluA2 subunit that makes them impermeable to calcium, a variety of young principal neurons express synaptic AMPA lacking GluA2. The timing of the switch from GluA2-lacking to GluA2-expressing synaptic AMPA varies according brain region and cell type. Within the rat somatosensory cortex layer 4 stellate cells appear to make this switch between postnatal days 7 and 8 (P7 and P8), while layer 2/3 pyramidal cells make the switch between P12 and P14 (Brill & Huguenard, 2008), and layer 5 pyramidal cells switch around P16 (Kumar et al., 2002). At the synapses between mossy fiber cells and CA3 pyramidal cells in the hippocampus, Ho et al. (2007) observed a transition from a population of mixed CP-AMPA and CI-AMPA

to primarily CI-AMPARs between 2 and 3 weeks postnatal. A postnatal switch from CP-AMPARs to CI-AMPARs has also been found at rat inner hair cells (Eybalin et al., 2004), and in the chicken forebrain (Migues et al., 2007), while in zebrafish Mauthner cells a change in AMPAR subunit composition appears to take place between 33 hours post-fertilization and 48 hours post-fertilization (Patten & Ali, 2007).

### **Role of CP-AMPARs in injury and disease**

CP-AMPARs have been strongly implicated in the neurological damage caused by a variety of brain injuries and disease processes that cause excess release of glutamate, a reduction in glutamate reuptake, or both. Excess exposure to extracellular glutamate initiates a number of processes toxic to neurons, described collectively as excitotoxicity (Lau & Tymianski, 2010). One of the primary ways in which glutamate excitotoxicity does so much neuronal damage is via overactivation of glutamate receptors such as CP-AMPARs, allowing extensive influx and accumulation of positive ions in the cytosol and overwhelming the neuron's ability to remove these ions and repolarize the neuronal membrane. Cytosolic overloads of calcium have been found to be particularly toxic, though despite extensive research all of the complex mechanisms responsible for this toxicity have yet to be elucidated. While glutamate-induced increases in postsynaptic calcium play a critical role in the molecular processes thought to underlie memory formation and maintenance, the concentration of calcium ions and time-course of ion influx must be tightly controlled. Excess calcium appears to initiate a number of intracellular cascades resulting in neurotoxic outcomes that cause cell death via apoptosis or necrosis. These include the generation of nitric oxide,

activation of calcium-sensitive proteases such as calpains, and uptake of calcium into mitochondria leading to generation of reactive oxygen species and release of apoptotic mediators such as cytochrome C, which can lead to activation of caspase cell-death pathways (Lau & Tymianski, 2010; Orrenius et al., 2003; Szydlowska & Tymianski, 2010; Weilinger et al., 2013). More recently, overload of cytosolic zinc ions has also been found to play a similar role in inducing excitotoxic cell death, often contributing to necrosis or apoptosis via the same pathways as calcium ions. CP-AMPARs are permeable to both zinc and calcium, meaning that their overactivation during excitotoxicity can contribute greatly to overload of cytosolic zinc and calcium, and consequent cell death (Kwak & Weiss, 2006; Sensi et al., 2009).

CP-AMPAR-linked excitotoxic damage appears to be at least partially responsible for the neuronal death and neurological deficits caused by oxygen- and nutrient-deprivation in the brain following a stroke, a heart attack or other ischemic event. Cerebral ischemia, the loss of blood flow to a portion of the brain, deprives neuronal tissue of the necessary oxygen and glucose to support neuronal function, leading to an increase in glutamate release into the extracellular space (Beppu et al., 2014; Davalos et al., 2000; Lau & Tymianski, 2010). Blockage or compression of blood vessels caused by a stroke or other trauma can cut off blood to a small or large portion of the brain, called focal ischemia, while global cerebral ischemia occurs when blood flow to the whole brain is cut off. Typically this happens during cardiac arrest or near drowning. Pyramidal neurons of the hippocampal CA1 region are particularly susceptible to the damage caused by the excess glutamate released during forebrain or global cerebral ischemia, selectively degenerating and then dying after a delay of several days.

Evidence suggests this is in part linked to an increase in CP-AMPA expression which makes the neurons more vulnerable to the excess extracellular glutamate. In the wake of global or forebrain ischemic insult, GluA2 expression is downregulated in the pyramidal CA1 neurons of the hippocampus, and there is an increase in inwardly rectifying excitatory postsynaptic currents (EPSCs) that can be blocked by NASPM. Furthermore, NASPM injected into the hippocampus after ischemic insult can partially protect the CA1 neurons from death (Kwak & Weiss, 2006; Lau & Tymianski, 2010; Liu & Zukin, 2007; Noh et al., 2005). There is also evidence to suggest that seizure or hypoxia-induced expression of CP-AMPA may be involved in the pathogenesis of some epileptic conditions, possibly dependent on the stage of brain development during which the initial trauma occurred (Cull-Candy et al., 2006; H. C. Prince et al., 2000; H. K. Prince et al., 1995).

CP-AMPA may significantly contribute to neurodegeneration in amyotrophic lateral sclerosis (ALS), a currently incurable disease in which progressive motor neuron degeneration leads to loss of muscle strength and control, paralysis, and eventual death. Some forms of ALS, known as familial ALS (fALS), run in families and in some cases are linked to known genetic mutations. However, the vast majority of cases are sporadic ALS (sALS), which arises in someone with no known family history of ALS, and in which there is often no genetic link yet identified. Despite intensive, ongoing research, the mechanisms and triggers underlying disease pathogenesis are still not well understood. Over twenty different mutations have been linked to fALS, and these account for only about half of fALS cases and very few sALS cases. Given the number of genetic and environmental factors already implicated in

disease progression and the heterogeneity of ALS clinical presentation, it is likely that different molecular pathways have greater or lesser importance as causative factors in the disease pathogenesis of different patient subgroups. Research to-date suggests ALS neurodegeneration is a complex interaction between genetic and molecular pathways, involving mechanisms that include mitochondrial dysfunction, oxidative stress, protein aggregation in the cytoplasm, and glutamate excitotoxicity (Kiernan et al., 2011; Shaw, 2005; Yamashita & Kwak, 2014).

Excitotoxicity has long been suspected as a mechanism in ALS motor neuron death due to the particular vulnerability of motor neurons to AMPA-mediated signaling in spinal cord culture (Kawahara et al., 2003). Initially, much research focused on the question of whether GluA2 expression was downregulated in ALS motorneurons, as that would imply the presence of CP-AMPA receptors and help explain the vulnerability to AMPAR-mediated excitotoxicity. Although results were mixed, the weight of the evidence suggested that the GluA2 subunit is present in these neurons, meaning that if CP-AMPA receptors are overexpressed it is likely not due to a lack of GluA2 (Kawahara et al., 2003; Vandenberghe et al., 2000). Consequently, Kawahara et al. (2004) turned their attention to investigating the role of GluA2 editing in ALS. Looking at motor neurons from five sALS patients they found evidence of reduced GluA2 mRNA editing efficiency, which suggests that CP-AMPA receptors might indeed be responsible for some excitotoxic motor neuron damage in ALS, but rather than lacking GluA2 these receptors could be incorporating unedited GluA2.

Hideyama et al. (2012) pursued the question of ALS motor neuron excitotoxicity due to impaired GluA2 editing on a somewhat larger scale, using spinal cord tissue and

motor neurons from 29 ALS patients who encompassed several different ALS phenotypes. To determine if GluA2 editing is different in ALS motor neurons versus motor neurons from control subjects they measured expression levels of ADAR2, the enzyme responsible for removing AMPAR calcium permeability via an edit to the mRNA of the GluA2 subunit at the Q/R site of the re-entrant loop of the M2 membrane region. They found that ADAR2 was downregulated in these neurons, and as might be expected, this downregulation correlated with a reduction in editing efficiency of GluA2 mRNA. This bolsters the suggestion that increased CP-AMPA expression may indeed be leading to excitotoxic death of motor neurons in many ALS cases of differing phenotypes. Furthermore, loss of ADAR2 activity in a motor neuron selective conditional knock-out mouse was found to lead to the slow death and degeneration of motor neurons, which could be rescued by expressing edited GluA2 (Hideyama et al., 2010). Interestingly, in the ADAR2-lacking motor neurons of these mice, the protein TDP-43 is found cleaved and aggregated in cytoplasmic inclusions. This pathology is a hallmark of ALS and is found in the majority of ALS cases, further implicating ADAR2 downregulation in ALS pathophysiology (Yamashita & Kwak, 2014). The clinical and therapeutic importance of understanding the role of CP-AMPA and excitotoxicity in ALS is highlighted by the fact that the only drug that has had even very moderate success at slowing disease progression is riluzole, a drug that inhibits glutamate release (Zinman & Cudkowicz, 2011).

## **Role of CP-AMPARS in drug addiction**

Animal model studies implicate CP-AMPARs in the neuronal plasticity underlying drug addiction. In response to drug exposure, CP-AMPAR levels have been found to increase in the ventral tegmental area (VTA) and the nucleus accumbens (NAc), two regions of the brain involved in motivation and reward circuitry (Wolf & Tseng, 2012). The increased receptor expression levels follow different time scales in the two regions, with an immediate response in the VTA. Saal et al. (2003) found that cocaine, amphetamine, nicotine, morphine and ethanol all increased excitatory synaptic input onto dopaminergic (DA) neurons of the VTA twenty-four hours after a single injection of the drug in question. Further research links this increase to the insertion of CP-AMPARs into the excitatory synapses onto DA neurons. A variety of cocaine exposure paradigms, including a single injection of the drug, have been shown to boost insertion of CP-AMPARs into the synapses of DA neurons of the VTA within twenty-four hours of drug administration in mice (Bellone & Luscher, 2006; Mameli et al., 2007) and rats (Argilli et al., 2008; Borgland et al., 2004). While this increase lasted only days following intraperitoneal injection regimens, a two-week self-administration regimen led to a potentiation of excitatory synapses onto the VTA that could still be detected months after withdrawal (Chen et al., 2008).

Elevated levels of calcium-permeable AMPARs are also detectable in the medium spiny neurons of the NAc during withdrawal from self-administered cocaine. In contrast to the VTA response, CP-AMPAR levels do not detectably increase in the NAc until several weeks after the start of withdrawal (Conrad et al., 2008; Mameli et al., 2009). At this point in withdrawal CP-AMPARs in the NAc appear to be involved in

mediating cue-induced cocaine cravings, which are frequently the cause of relapse for recovering addicts (Pickens et al., 2011). This avenue of research suggests that CP-AMPARs offer a potential druggable target to help recovering addicts avoid relapses. In an animal model, both directly blocking CP-AMPAR transmission (Conrad et al., 2008) and preventing CP-AMPAR accumulation during withdrawal (Loweth et al., 2014) reduced cocaine-seeking behavior.

### **Use of endogenous polyamines and neurotoxins to target CP-AMPARs**

A number of polyamine-containing neurotoxins found in insect venoms have some degree of selectivity for CP-AMPARs, and synthetic analogues of these toxins have provided a means for pharmacologically distinguishing subtypes of ionotropic glutamate receptors. Polyamines are small molecules that play an interesting and varied role in eukaryotic cellular biology, and have been found to be involved in regulating a number of cellular functions including cell growth and death, protein synthesis, and signaling through ion channels in the cell membrane (Li et al., 2007; Stromgaard & Mellor, 2004). The endogenous polyamines spermine and spermidine are known to interact with several ionotropic glutamate receptors including AMPARs, kainate receptors, and NMDARs.

These polyamines block active CP-AMPARs and calcium-permeable kainate receptors (CP-KARs) when applied extracellularly (Washburn & Dingledine, 1996), and block them intracellularly as well, in a voltage-dependent fashion. This intracellular block

is in fact responsible for the inwardly-rectifying property of CP-AMPA receptors and CP-KARs. As the neuronal membrane depolarizes, intracellular polyamines block the ion channel, preventing cations from flowing down their concentration gradient and out of the cell (Bowie & Mayer, 1995; Stromgaard & Mellor, 2004). This polyamine blockage is possible due to the presence of the glutamine, as opposed to the positively charged arginine, at the Q/R site in the re-entrant loop of the M2 membrane region of CP-AMPA receptors and CP-KARs. While endogenous spermine has been shown to potentiate both NMDA receptors (Mony et al., 2009) and kainate receptors (Mott et al., 2003), this interaction most likely revolves around spermine stabilization of either the amino-terminal domain interface or the ligand-binding domain interface, rather than the open channel-block which is the defining interaction between ionotropic receptors and the polyamine toxins.

Polyamine toxins found in spider and wasp venoms exploit one aspect of this open-channel blocking interaction with ion channels, but instead of normal ion channel regulation these toxins can block some channels completely, leading to paralysis. The first polyamine toxin structure to be characterized was the orb weaver spider venom argitoxin-636 (ArgTX-636), which was characterized in 1986. The structure of Joro spider toxin (JSTX-3) was next to be characterized, followed by a number of other spider toxins, as well as the Egyptian digger wasp venom philanthotoxin (PhTX-433). ArgTX-636, JSTX-3, PhTX-433, and PhTX-343 have been shown to act as open-channel blockers that selectively bind to the intrinsic ion channel of glutamate-bound calcium-permeable AMPA and kainate receptors. That is, these toxins block receptors

that are in the process of receiving glutamatergic neurotransmission (Stromgaard & Mellor, 2004).

The historical use of these polyamine toxins to target receptors with specificity is somewhat complex. The range of measured IC<sub>50</sub> values for polyamine toxins applied to CP-AMPARs has generally been given as somewhere between 30 nM and 3 μM (Brackley et al., 1993; Jackson et al., 2011). However, molecules in this pharmacological class are also known to antagonize both NMDARs and nAChRs, particularly at higher concentrations, though reports on the potency of such compounds for these two receptor classes are very mixed. Some studies have even reported that certain polyamine toxins have similar IC<sub>50</sub> values for both NMDARs and CP-AMPARs, typically in the nM to single μM range.

This variability of IC<sub>50</sub> values appears to be due to the employment of a range of experimental conditions, cell types, and the use of endogenous versus heterologous receptors, all of which affect the subunit make-up of the receptor, and hence sensitivity to polyamine toxins. An early study by Brackley et al. (1993) tested two different polyamine toxins on glutamate receptors, using two different approaches to receptor expression in *Xenopus* oocytes. They found that when rat brain RNA was injected into oocytes, for both non-NMDA glutamate receptors and NMDARs the IC<sub>50</sub> of ArgTx-636 was sub-micromolar. The IC<sub>50</sub> of PhTx-343 for non-NMDA glutamate receptors was also sub-micromolar, while for NMDARs it was 2.5 μM. However, oocytes expressing only GluA1 RNA were much less sensitive to blockage by either polyamine, with both toxins producing an IC<sub>50</sub> of around 3 μM. For oocytes injected with only NMDAR1, ArgTx-636 still had a sub-micromolar IC<sub>50</sub>, while PhTx-343 had

an  $IC_{50}$  over 2  $\mu M$ . Oocytes expressing GluA1 and GluA2 together were essentially insensitive to blockage by either toxin, with both producing  $IC_{50}$ s of around 300  $\mu M$ . A later study also using whole rat brain RNA provided supporting evidence that non-NMDA glutamate receptors are more sensitive to PhTx-343 than other possible targets. When receptors heterologously expressed in *Xenopus* oocytes were treated with the PhTX-343 at -80 mV, an  $IC_{50}$  of 0.46  $\mu M$  was found for AMPARs, and an  $IC_{50}$  of about 2  $\mu M$  was found for NDMARs. An  $IC_{50}$  of approximately 16  $\mu M$  was found for nAChRs, which were endogenously expressed on TE671 cells held at -100 mV. The selectivity for AMPARs was dramatically improved with the modified compound PhTX-83, which had an  $IC_{50}$  of 32 nM (Mellor et al., 2003; Stromgaard & Mellor, 2004).

These somewhat mixed results are likely attributable to several factors, including the use of a heterologous expression system that appears to express endogenous glutamate receptor subunits capable of interacting with the heterologous subunits to some degree (Schmidt & Hollmann, 2008; Schmidt et al., 2009; Soloviev & Barnard, 1997). Additionally, in the preceding examples kainate was used to activate non-NMDA glutamate receptors prior to polyamine toxin block. Jackson et al. (2011) later found that philanthotoxin is much more effective at blocking CP-AMPARs treated with glutamate than those treated with kainate. They also found that the presence of transmembrane AMPAR regulatory proteins (TARPS) increases the potency of PhTx-433 at blocking CP-AMPARs. This suggests that endogenous AMPARs expressed on neurons that also natively express TARP proteins will have more sensitivity to blockage by polyamine toxins than heterologously expressed recombinant AMPARs.

When testing polyamine toxin sensitivity on oocytes expressing whole rat brain RNA (Brackley et al., 1993; Mellor et al., 2003) or on cerebellar granule neurons (CGNs) from GluA2 knock-out mice (Jackson et al., 2011), CP-AMPARs were not pharmacologically isolated from CP-KARs. However in the CGNs CP-AMPARs likely heavily outnumbered CP-KARs, as the lack of GluA2 would make all AMPARs calcium-permeable, while kainate receptors were presumably present in normal ratios of calcium-permeable and impermeable receptors. In a paper that provides a more direct comparison of polyamine toxin effects on CP-AMPARs and CP-KARs, Bähring and Mayer (1998) studied the response of homomeric CP-KARs consisting of GluK2(Q) subunits (also known as GluR6(Q) subunits) and homomeric GluA1 CP-AMPARs to PhTX-343 block. While they found an  $IC_{50}$  of 60 nM at -60 mV for GluK2 homomers using domoic acid, they found GluA1 homomers to be even more sensitive to PhTX-343 block. The GluA1 homomers were almost entirely blocked by 30 nM of the philanthotoxin at -60 mV, using glutamate as an agonist, suggesting that while both CP-KARs and CP-AMPARs are sensitive to philanthotoxin block under the correct conditions, CP-AMPARs are preferentially targeted. When Blaschke et al. (1993) treated CP-AMPARs or GluK2(Q) CP-KARs with 0.5  $\mu$ M JSTX-3, they found both receptors ranged from 80% blocked to nearly 100% blocked. The relatively high dose of toxin used may have prevented differences in receptor sensitivity from being revealed.

Naphthyl acetyl spermine (NASPM) was originally synthesized as an analogue of JSTX-3, to have more specificity for CP-AMPARs (Stromgaard & Mellor, 2004). While a few studies have used NASPM to target both CP-AMPARs and CP-KARs, in these

cases the authors used relatively high concentrations of 200  $\mu\text{M}$  (Sun et al., 2009) to 300  $\mu\text{M}$  NASPM (Ogoshi & Weiss, 2003; Yin et al., 2002). Koike et al. (1997) found NASPM be a specific blocker of CP-AMPARs when tested on hippocampal neurons with a strong inwardly rectifying response to kainate and high calcium-permeability, due to expression of AMPARs containing only GluA1 and GluA4 subunits (Iino et al., 1996). They found a NASPM  $\text{IC}_{50}$  of 0.33  $\mu\text{M}$  at -60 mV for these neurons. In contrast, hippocampal neurons with a slight outwardly rectifying response to kainate and low calcium permeability were insensitive to NASPM block. Currently, NASPM is the de facto standard used as a CP-AMPAR-specific ligand (Camire & Topolnik, 2014; Gong et al., 2011; Hainmuller et al., 2014; Loweth et al., 2014; McCutcheon et al., 2011; Studniarczyk et al., 2013; White et al., 2015). For this reason, NASPM was selected to be the primary model for the targeting ligand of a novel nanoprobe designed and synthesized in the Chambers lab for the purpose of labeling endogenous CP-AMPARs in live neurons with a minimally perturbing, fluorescent tag.

### **Nanoprobe for labeling CP-AMPARs**

The Chambers lab has developed a novel photocleavable nanoprobe (Figure 2) for labeling endogenous CP-AMPARs in live cells with minimal disruption to native receptor activity. This nanoprobe is a ligand-targeted molecular tag designed to covalently label native membrane-bound receptors with a non-perturbing, fluorescent marker that then allows observation of these receptors using standard epifluorescence microscopy. To achieve CP-AMPAR specificity, the ligand portion of the probe was designed to capitalize on the pharmacology of the polyamine toxin molecules Joro

spider toxin, argiotoxin, philanthotoxin-433 and, most structurally similar, the synthetic CP-AMPA blocker NASPM (Brackley et al., 1993; Stromgaard et al., 1999; Stromgaard & Mellor, 2004; Yoneda et al., 2001). Once nanoprobe has been applied, the ligand can be cleaved, leaving only the fluorescent tag covalently-bound to the receptor (Vytla et al., 2011). As the nanoprobe requires no genetic manipulation and uses a small molecule dye as the fluorescent label, this system offers the opportunity to observe receptor location and activity without the potentially confounding effects of genetic overexpression or of labeling with a large macromolecule such as an antibody or fluorescent protein.

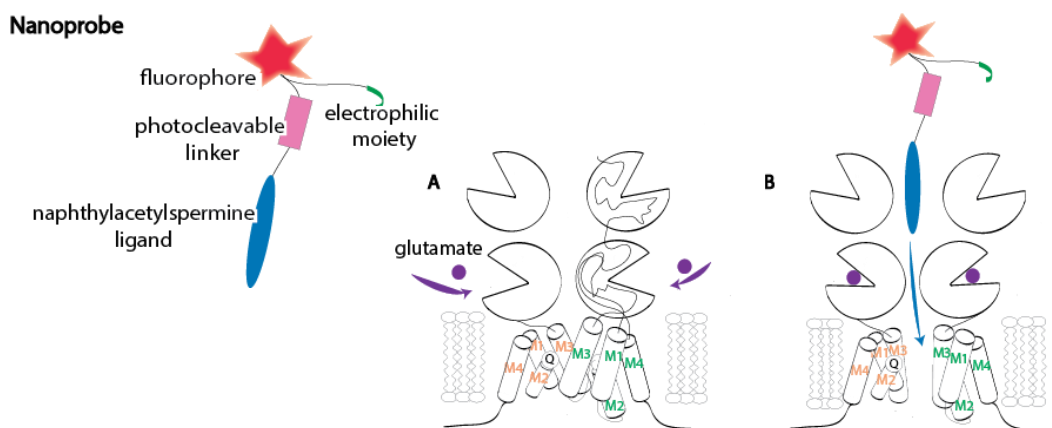


**Figure 2: Nanoprobe design and labeling of active CP-AMPA receptors.** The nanoprobe has a NASPM ligand (blue oval) to target CP-AMPA receptors, a fluorophore (red star) so targeted receptors can be visualized, and an electrophilic moiety (green hook) to covalently bond with nucleophiles on the CP-AMPA receptor surface. Once this has happened UV light can cleave the ligand at the photocleavable linker (pink box). **A and B, labeling of activated CP-AMPA receptors with nanoprobe.** Two of the four subunits are shown. Prior to glutamate binding (A) the intrinsic ion channel is closed. (B) After glutamate binds, the intrinsic ion channel opens and the NASPM-derived ligand (blue oval) can enter the open channel. This brings the electrophilic moiety (green hook) close enough to the receptor surface to covalently bond an available nucleophile.

Due to the NASPM-derived ligand, this tri-part nanoprobe is designed to be selective for active CP-AMPA receptors. After binding glutamate, the transmembrane helices move to

open the channel so that ions can pass through. When binding takes place, the ligand-binding domain closes around the glutamate, and it is thought that this movement pulls the M3 helix up and away from each other, unblocking the channel (Dong & Zhou, 2011). After the nanoprobe ligand has moved into the open channel (see Figure 2), the electrophilic moiety on the nanoprobe is brought into close proximity with the surface of the receptor, making it possible for the electrophile to form a covalent bond with a nucleophilic amino acid on the surface of the receptor. Once that bond has formed the ligand can be cleaved using UV light, thus allowing the receptor to return to its normal, unbound state while leaving the fluorescent part of the probe bound to the receptor via the electrophilic moiety (Figure 3).

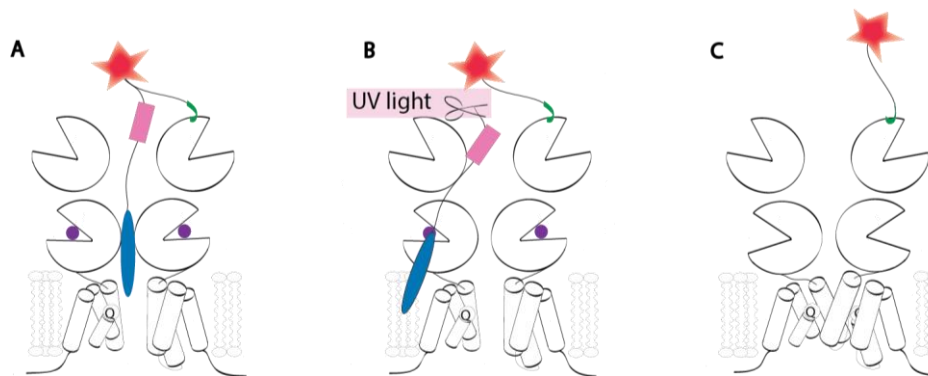


**Figure 3: Photocleaving ligand after nanoprobe labeling leaves probe fluorophore bound to unperturbed CP-AMPA. A)** The NASPM-derived ligand (blue oval) interacts with the open channel of the active CP-AMPA while glutamate (purple circle) is bound to the receptor subunits. This brings the electrophilic moiety (green hook) in close proximity to the CP-AMPA, allowing it to covalently bind an available nucleophile on the receptor surface. **B)** UV light is used to cut the photocleavable linker (pink box), and the ligand washes away while the fluorophore (red star) remains bound to the receptor. **C)** The unblocked receptor returns to normal activity, now labeled with a fluorescent tag.

# CHAPTER 3

## RESEARCH DESIGN AND METHODS

### Aim 1: Whole cell patch clamp electrophysiology

The goal of aim 1 is to use whole cell patch clamp electrophysiology to test the labeling of CP-AMPARs with nanoprobe by recording changes in glutamate-evoked current through heterologously expressed GluA1-L497Y homomultimers during, pre- and post- nanoprobe labeling.

To evaluate how nanoprobe interacts with CP-AMPARs, HEK293T cells will be transfected with GluA1-L497Y-pIRES2-eGFP cDNA using liposomal delivery. After the transfected HEK cells express GFP-tagged GluA1 homomers, glutamate-evoked current through these receptors will be recorded before and after nanoprobe treatment, allowing us to measure the effect of nanoprobe on CP-AMPAR function. HEK293T cells will be plated on glass coverslips treated with polylysine, grown at 5% CO<sub>2</sub> and 37 °C, and at 70% confluency cells will be transfected with bicistronic vector GluA1-L497Y-pIRES2-eGFP (Nagarajan et al., 2001). The GluA1-L497Y subunit is a non-desensitizing variant of the GluA1 subunit, used here to slow desensitization and facilitate data collection. AMPAR desensitization occurs after a period of ongoing agonist exposure, resulting in the closure of the intrinsic ion channel while agonist is still bound to the receptor (Gouaux, 2004; Mitchell & Fleck, 2007). By reducing desensitization we can extend the time during which data on AMPAR current can be collected.

One to three days post-transfection green cells will be located and then subjected to whole cell patch clamp electrophysiology. After washout of residual media, whole cell patch configuration will be established, holding cells at -70 mV. Extracellular solution (ECS) will be continuously perfused onto the coverslip unless otherwise noted, while drug compounds will be delivered to the patched cell by local perfusion, as in Figure 4.

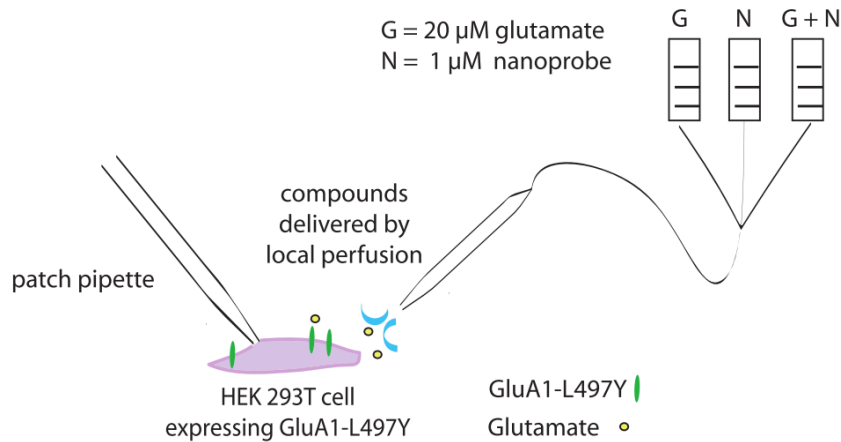


**Figure 4: Nanoprobe application during whole cell patch clamp electrophysiology of HEK293T cells expressing CP-AMPA receptors.** HEK293T cells transfected with GluA1-L497Y-pIRES2-eGFP will express CP-AMPA receptors consisting of GluA1 homomers. Green cells will be patched to measure current through these receptors, and then cells will be perfused with either glutamate alone, nanoprobe alone, or glutamate and nanoprobe together to measure the effect of nanoprobe on glutamate response.

A baseline glutamate response will first be measured by delivering three 1 second pulses of 20  $\mu$ M glutamate, each delivered 1 minute apart. Next, ECS perfusion will be turned off as a combined solution of 20  $\mu$ M glutamate and 1  $\mu$ M nanoprobe is washed on for 1 min, after which ECS perfusion will be started up again. After washing the coverslip for 1 minute to remove residual nanoprobe and glutamate, a 1 second pulse of 20  $\mu$ M glutamate will be delivered to probe the ability of the GluA1 channels to open in response to glutamate and allow ionic current to flux into the cell.

Fifteen seconds later, another 1 sec pulse of 20  $\mu\text{M}$  glutamate will be delivered in combination with a 15 second exposure to 380 nm light, which should release the NASPM-derived ligand, unblocking the channels and restoring glutamate-evoked ionic current into the cell. Following ligand-release, three 1 second pulses of 20  $\mu\text{M}$  glutamate will be delivered, each 1 minute apart to determine the average glutamate response post-treatment. The peaks of the initial three glutamate responses that were recorded prior to treatment with nanoprobe will be averaged, and maxima of glutamate-evoked responses later in the experiment will be normalized to this average baseline response. Figures 5 and 6 illustrate the predicted glutamate-evoked current in response to perfusion with glutamate alone and in combination with nanoprobe.

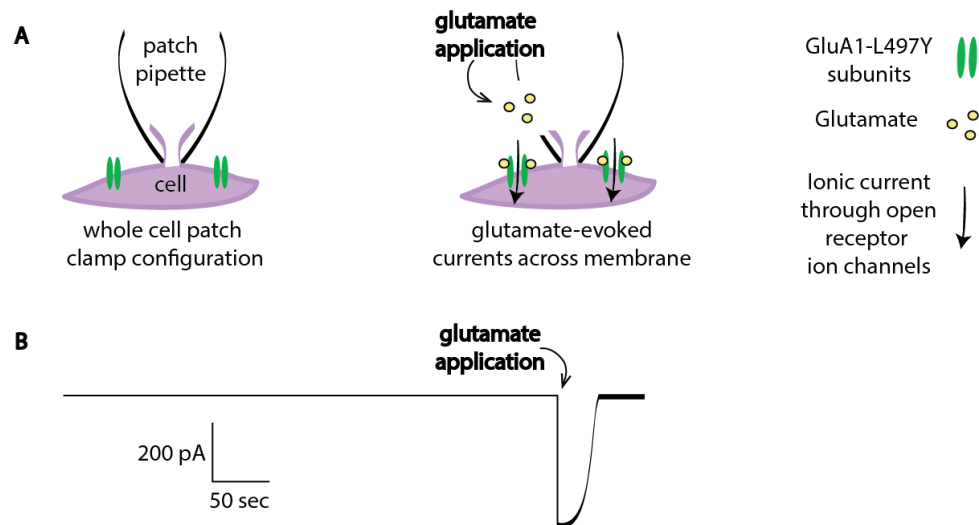


**Figure 5: CP-AMPA glutamate response recorded with whole cell patch clamp electrophysiology.** HEK293T cells expressing CP-AMPA receptors consisting of GluA1-L497Y homomers will be patched, held at -70 mV and perfused with glutamate. **A)** A cartoon illustration of whole cell patch clamp configuration. A pipette is patched onto an HEK cell that expresses CP-AMPA receptors. The cell membrane is perforated where the pipette tip meets the membrane so that current through the CP-AMPA receptors of the cell can be measured. When glutamate is perfused onto the cell, the CP-AMPA receptors bind the glutamate, opening the intrinsic ion channel and allowing positive ions to flux into the cell. **B)** A cartoon illustration of a typical glutamate-evoked current, measured in picoamps (pA) over time.

To evaluate the use-dependency of nanoprobe, these results will be compared to glutamate-evoked responses in cells treated with 1  $\mu$ M of nanoprobe alone. In these control experiments the initial three pulses of 20  $\mu$ M glutamate will be delivered to establish an average baseline response following the same protocol as used in the initial experiment. However, those three pulses will be followed by a 1 min application of 1  $\mu$ M nanoprobe alone, rather than a combined treatment of glutamate and nanoprobe together. After treatment with nanoprobe alone, the protocol will be identical to the previously described experiment. ECS perfusion will be re-established

and the coverslip will be washed for 1 min, two pulses of glutamate will then be delivered 15 seconds apart, the second one accompanied by a 15 second exposure to UV light, and three final pulses of glutamate will be delivered.

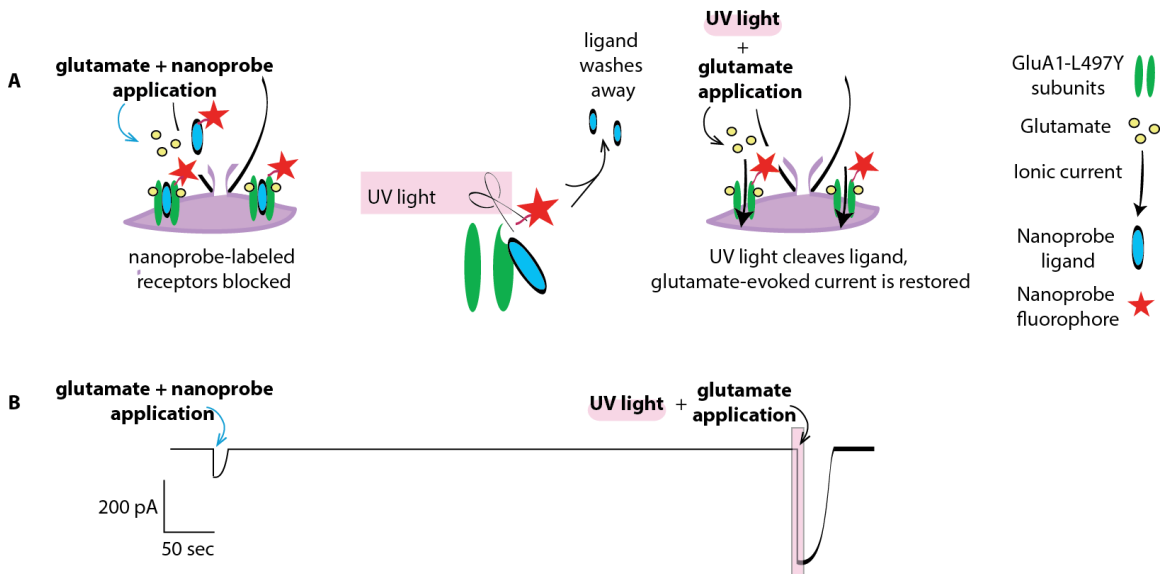


**Figure 6: Nanoprobe block of CP-AMPA glutamate response, and release of block via photolysis, recorded with whole cell patch clamp electrophysiology. A)** After perfusion with glutamate and nanoprobe, CP-AMPA receptors bind the glutamate, opening the intrinsic ion channels of the receptors. This allows nanoprobe ligand to interact with the ion channels, blocking glutamate response and bringing the nanoprobe fluorophore into contact with the CP-AMPA surface where it covalently binds. UV light cleaves the ligand, restoring normal glutamate response to receptors now labeled with fluorophore. **B)** A cartoon illustration of predicted glutamate-evoked current in response to treatment with nanoprobe and glutamate combined, and in response to glutamate treatment after ligand is cleaved with UV light. Current is measured in picoamps (pA) over time.

## **Aim 2: Imaging co-labeled endogenous receptors**

The goal of aim 2 is to use fluorescent imaging to evaluate nanoprobe labeling of glutamate receptors endogenously expressed in hippocampal neurons by co-labeling nanoprobe-treated neurons with traditional antibodies to AMPAR and synaptic targets.

To evaluate nanoprobe labeling of endogenous glutamate receptors, fluorescent imaging will be used to compare the locations of nanoprobe-labeled receptors to the locations of proteins labeled with synaptic and AMPAR antibodies. Primary dissociated hippocampal cultures will be prepared from embryonic day E18-E20 Sprague-Dawley rat embryos. Hippocampi will be isolated, trypsinized and cultured for 14-24 days on polylysine-treated coverslips, grown in serum-containing medium at 5% CO<sub>2</sub> and 37 °C, and fed 200 uL of media about every five days. All animal care and experimental protocols were approved by the Animal Care and Use Committee at University of Massachusetts Amherst, Amherst, MA, USA.

As an initial step towards visualizing CP-AMPARs at active synapses via nanoprobe labeling of native neuronal receptors, coverslips of live dissociated hippocampal cultures will be imaged before and after treatment with nanoprobe. Coverslips will be washed with 3 times with ECS, imaged to establish background fluorescence, incubated with nanoprobe, washed 3 more times with ECS and imaged again.

After using live imaging experiments to develop initial treatment and imaging parameters for nanoprobe labeling of neurons, coverslips will be labeled with both nanoprobe and fluorescent antibodies to evaluate probe colocalization with synaptic

and AMPAR proteins. Dissociated hippocampal neurons will be treated with a range of nanoprobe concentrations, fixed, and stained with an antibody to either AMPA receptors generally, to GluA1 specifically, or to the synaptic protein synapsin. Anti-AMPAR and anti-GluA1 will label both synaptic and extra-synaptic AMPARs, and synapsin will label synapses.

To visualize nanoprobe colocalization with AMPA receptors, coverslips of dissociated hippocampal culture will be treated with either the polyclonal Santa Cruz Biotech pan-AMPAR antibody at 1:200 dilution or with the Millipore Anti-GluR1-NT RH 95 monoclonal antibody at 1:1000 dilution. Coverslips will be washed with ECS three times, treated with nanoprobe, and fixed in 4% paraformaldehyde for at least 10 min. Following cell fixation, coverslips will be washed three times with PBS, and treated with permeabilizing or non-permeabilizing blocking buffer containing goat serum in preparation for labeling with primary antibody.

Permeabilizing blocking buffer will be used during treatment with polyclonal pan-AMPAR antibody to allow the antibody access to both extracellular and intracellular epitopes. Anti-GluA1 treated coverslips will be incubated with either permeabilizing or non-permeabilizing blocking buffer. The anti-GluA1 antibody targets the n-terminus of the GluA1 subunit, which is located on the extracellular portion of the protein, so use of non-permeabilizing blocking buffer will label only GluA1-containing AMPARs that are still surface-expressed at the time of fixation. Use of permeabilizing blocking buffer will allow us to visualize both externally expressed and internalized GluA1 subunits.

After labeling with primary antibody coverslips will be washed with PBS and treated with secondary antibody. Anti-GluA1 coverslips will be treated with the Thermo Scientific Goat Anti-Mouse IgG DyLight 488 secondary antibody, while pan-AMPA treated coverslips will be labeled with 488 DyLight goat anti-rabbit secondary antibody. Following antibody labeling coverslips will be washed again with PBS, dried, mounted with ProLong Gold antifade and sealed.

To visualize nanoprobe colocalization with synapses, nanoprobe-treated coverslips will be labeled with the monoclonal antibody from Cell Signaling for the synaptic marker synapsin-1 (D12G5) XP, product number 5297. Dissociated hippocampal cultures will be washed with ECS three times and treated with nanoprobe. As with anti-GluA1 and pan-AMPA treated cultures, coverslips will be fixed in 4% paraformaldehyde for at least 10 min, washed three times with PBS, and treated with permeabilizing blocking buffer containing goat serum in preparation for labeling with primary antibody. After labeling with anti-synapsin-1, coverslips will be washed with PBS, treated with 488 DyLight goat anti-rabbit secondary antibody, and washed again with PBS. Following antibody labeling, coverslips will be dried, mounted with ProLong Gold antifade and sealed.

To further evaluate nanoprobe specificity in labeling of native neuronal receptors, dissociated hippocampal cultures will also be treated with nanoprobe in combination with either 25 $\mu$ M of the non-NMDAR glutamate receptor antagonist DNQX, a stoichiometric concentration of non-liganded nanoprobe, or 20 $\mu$ M glutamate, prior to being fixed and stained with primary antibody. If nanoprobe is specifically targeting active CP-AMPA receptors, DNQX should reduce nanoprobe labeling while glutamate should

increase labeling and colocalization with anti-GluA1 or pan-AMPA antibody. Treatments with non-liganded nanoprobe will allow us to visualize off-target labeling due to interactions of the nanoprobe electrophile with non-CP-AMPA nucleophiles on the cell membrane.

### **Aim 3: Imaging and tracking nanoprobe-labeled receptors** **on live neurons**

The goal of aim 3 is to use nanoprobe to detect endogenously expressed CP-AMPA during the course of neuron development. Live neuronal cultures will be imaged before and after labeling with nanoprobe in young dissociated cultures (DIV 1-2) and in maturing cultures (DIV 14-17).

To label and track the movement of endogenous CP-AMPA of live hippocampal neurons, primary dissociated hippocampal cultures will be incubated with nanoprobe and imaged live using confocal fluorescent microscopy. Hippocampi will be isolated from embryonic day E18-E20 Sprague-Dawley rat embryos, trypsinized and cultured for either 1-2 days or 14-17 days on polylysine-treated coverslips, grown in serum-containing medium at 5% CO<sub>2</sub> and 37 °C, and fed 200 uL of media about every five days.

## **Dose-dependent labeling of live neurons with nanoprobe**

Prior to imaging and tracking CP-AMPARs on live cells, the appropriate nanoprobe concentration for live labeling will be determined. During prior imaging experiments that primarily focused on fixed cell imaging, it was difficult to establish a consistently effective concentration. As previously mentioned, the reported IC<sub>50</sub> values for this class of blockers range from 30 nM to 3 μM (Brackley et al., 1993; Jackson et al., 2011) and much of this variation seems attributable to differences in tissue culture and experimental conditions. Thus, during our live labeling experiments a similar range of nanoprobe concentrations will be tested to optimize labeling while attempting to maintain specificity.

To determine the optimal nanoprobe concentration for use in labeling live cells, a range of concentrations from 100 nM to 3 μM will be tested on DIV 14-17 neurons. We chose 100 nM as our low concentration because previous experiments with 30 nM resulted in no detectable fluorescence accumulation. Coverslips will be washed 3 times with extracellular solution (ECS), imaged to establish background fluorescence, and then treated with 100 nM nanoprobe in ECS for 5 minutes. After this incubation period with a low concentration of nanoprobe, the coverslips will be gently washed 3 times with ECS and imaged again. Finally, the same region of the coverslip will be used to assay a higher concentration of nanoprobe, independently either 300 nM, 1 μM, or 3 μM in ECS. A 5 minute incubation in the higher concentration of nanoprobe will be followed by three washes with ECS prior to resuming imaging. Fluorescence intensity of tissue labeled at the higher probe concentration will be compared to

fluorescence intensity at the 100 nM concentration and both will be compared to background fluorescence prior to any labeling.

### **Co-incubation with competitor molecules**

To test the specificity of nanoprobe for CP-AMPARs on live neurons, probe will be applied to DIV 14-17 neurons while co-treating the coverslips with the non-fluorescent competitor molecules NASPM or DNQX. Co-treatment with a stoichiometric concentration of NASPM will test for specificity to NASPM-sensitive targets, presumably primarily CP-AMPARs. As NASPM interacts with the CP-AMPAR ion channel pore of active receptors in the same way that the nanoprobe ligand is designed to interact with those ion channel pores, NASPM should prevent interaction between nanoprobe and CP-AMPARs. Co-treatment with 10  $\mu$ M DNQX will test for specificity to AMPARs and kainite receptors, as DNQX blocks the glutamate-binding site of those receptors. Lack of glutamate-binding should prevent channel opening, thus also preventing nanoprobe interaction with the open CP-AMPAR ion channel. Together these co-incubations will help us determine if nanoprobe is indeed targeting NASPM-sensitive glutamate receptors.

To establish background fluorescence, each coverslip will be washed 3 times with ECS and imaged prior to any treatments with nanoprobe or competitor molecules. Each coverslip will then be simultaneously co-treated with 300 nM nanoprobe and a competitor molecule, washed 3 times with ECS, and imaged again. Finally, coverslips will be treated with 300 nM nanoprobe alone, washed 3 times with ECS and imaged. Fluorescence intensity of tissue labeled in the presence of nanoprobe alone will be

compared to the fluorescence intensity of the same location when treated with both nanoprobe and a competitor, and both will be compared to background fluorescence.

To evaluate nanoprobe specificity when applied to neurons shortly after plating, DIV 1-2 neurons will be treated with nanoprobe in conjunction with the non-NMDAR glutamate receptor antagonist DNQX, and again without the presence of DNQX. Coverslips of DIV 1-2 neurons will be washed with ECS, treated with 10  $\mu$ M DNQX in conjunction with 300 nM nanoprobe, washed again, imaged, treated with 300 nM nanoprobe alone, washed and imaged again. Fluorescent labeling of tissue treated with nanoprobe alone will be compared to labeling in the presence of DNQX.

### **Tracking movements of nanoprobe-labeled receptors in young and maturing cultures**

One of the motivations for the development of a traceless, chemical-based method to label CP-AMPARs was to observe minimally perturbed receptor movements in live neurons. To visualize labeling and trafficking of endogenous receptors on live neurons, we will record time-lapse images of live neurons labeled with nanoprobe. Coverslips of DIV 14-17 neurons will be washed with ECS, incubated with 300 nM nanoprobe for 5 min in the dark, exposed to 405 nm light for photolysis of the nitroindoline, washed again, and imaged to compile a time-series. To visualize trafficking of CP-AMPARs in earlier stages of neuron development, we will follow the same washing and labeling steps on DIV 1-2 neurons.

## **Co-incubation with mitochondrial label**

To determine if nanoprobe labeling overlaps with mitochondrial locations in DIV 1-2 neurons, coverslips will be co-treated with both nanoprobe and the mitochondrial label MitoTracker Green FM from Cell Signaling Technology. The neurons will be washed with ECS, treated with nanoprobe and washed again, then incubated with 500 nM MitoTracker for 1 minute, washed with ECS and imaged again.

# CHAPTER 4

## EXPECTED RESULTS

### Aim 1: Whole cell patch clamp electrophysiology

The goal of aim 1 is to use whole cell patch clamp electrophysiology to test the labeling of CP-AMPA receptors with nanoprobe by recording changes in glutamate-evoked current through heterologously expressed GluA1-L497Y homomultimers during, pre- and post- nanoprobe labeling.

If the nanoprobe behaves as an open-channel blocker as designed, I would predict that during the treatment with glutamate and nanoprobe together there will be a loss of current as the nanoprobe ligand enters the open channels and blocks ion flow (Figure 6). Once the nanoprobe ligand has entered a channel, it should bring the electrophilic arm of the probe into proximity with nucleophiles on the surface of the receptor, leading to a covalent interaction that anchors the nanoprobe within the ion channel. I would expect this to be demonstrated by a continued channel block even after excess nanoprobe has been washed away and a new pulse of glutamate has been delivered to re-open the channels. Finally, if the ligand is photocleavable as expected, the application of UV light should cleave the ligand from the rest of the molecule, allowing the ligand to wash away. Without ligand blocking the channels glutamate-evoked current should be restored (Figure 6), which I would expect following application of UV light in conjunction with glutamate.

In contrast, when nanoprobe alone is applied to a patched cell, I would predict that glutamate-evoked responses following nanoprobe treatment will be the same as the pre-treatment glutamate pulses. Nanoprobe ligand should be unable to enter the channels of inactive CP-AMPARS, so I would expect the nanoprobe to simply remain in the bath until washed away, after which the channels should open in response to glutamate and pass ionic current as they normally would (Figure 5).

### **Aim 2: Imaging co-labeled endogenous receptors**

The goal of aim 2 is to use fluorescent imaging to evaluate nanoprobe labeling of glutamate receptors endogenously expressed in hippocampal neurons by co-labeling nanoprobe-treated neurons with traditional antibodies to AMPAR and synaptic targets.

If nanoprobe labels CP-AMPARs as it is designed to do, I would expect nanoprobe to largely colocalize with pan-AMPAR and GluA1 antibodies, as both antibodies will target all AMPARs, including CP-AMPARs. As these antibodies should label all calcium-impermeable AMPARs too, I would expect a large population of receptors to be labeled with antibody but not co-labeled by nanoprobe. I would also expect to see some overlap between nanoprobe labeling and the antibody for the pre-synaptic protein synapsin-1, though again I would expect the antibody labeling to be much more widespread than nanoprobe labeling, as synapsin-1 is found at both glutamatergic and GABAergic synapses. Synapses expressing CP-AMPARs would only be a small subset of all synapses labeled by anti-synapsin 1.

The pharmacological treatments (glutamate, DNQX) applied in conjunction with nanoprobe should alter the amount of probe that colocalizes with AMPAR and synapsin antibodies, as well as the total amount of probe labeling visible on treated neurons. When neurons are treated with nanoprobe alone, I would expect to see labeling only at active synapses, as availability of glutamate-bound CP-AMPARs would be restricted to those sites. A global treatment of glutamate would theoretically make all surface-expressed CP-AMPARs available for nanoprobe labeling, resulting in more abundant probe labeling and more colocalization with anti-AMPAR antibodies. Thus, following co-application of glutamate and nanoprobe to neurons, I would expect to see more widespread nanoprobe labeling of CP-AMPARs at active synapses and CP-AMPARs at extrasynaptic sites. In contrast, I would expect neurons treated with DNQX and nanoprobe together to have reduced probe labeling. DNQX blocks the glutamate-binding site of non-NMDAR glutamate receptors, which should prevent CP-AMPARs from binding glutamate and thus reduce the number of CP-AMPARs with open ion channels available for interaction with nanoprobe.

As non-liganded nanoprobe lacks the NASPM-derived ligand to enable specific interaction with CP-AMPARs, I would expect neurons treated with this compound to have greatly reduced fluorescent labeling when compared to neurons treated with fully liganded probe. There may be some labeling as a result of interactions between non-CP-AMPAR nucleophiles on the cell membrane and the electrophile on the non-liganded probe. Non-liganded nanoprobe will allow us to visualize the extent of this off-target labeling.

### **Aim 3: Imaging and tracking nanoprobe-labeled receptors** **on live neurons**

The goal of aim 3 is to use nanoprobe to detect endogenously expressed CP-AMPARs during the course of neuron development. Live neuronal cultures will be imaged before and after labeling with nanoprobe in young dissociated cultures (DIV 1-2) and in maturing cultures (DIV 14-17).

If nanoprobe labels CP-AMPARs in live neuronal culture as expected, I predict an increase in punctate fluorescent labeling on a subset of neurons following treatment with probe. Given that the reported range of  $IC_{50}$  values for this pharmacological class is 30 nM to 3  $\mu$ M (Brackley et al., 1993; Jackson et al., 2011), I would expect effective labeling to occur somewhere within this range, likely on the low end. While the  $IC_{50}$  values for polyamine toxins at CP-AMPARs and other receptors are covered in greater depth in the introduction, most significantly Koike et al. (1997) found an  $IC_{50}$  of 0.33  $\mu$ M for NASPM blockage of CP-AMPARs. As nanoprobe ligand is derived from NASPM, I would expect the probe molecule to have a similar  $IC_{50}$ , suggesting that a dose in the range of 300 nM to 1  $\mu$ M should be sufficient to effectively label a majority of CP-AMPARs.

As discussed in the introduction, CP-AMPARs are known to be involved in some forms of synaptic plasticity, and to be abundant on some neurons in early stages of development. Thus I would expect to see labeling on both older, synaptically active neurons undergoing spinogenesis (DIV 14-17) and on younger neurons shortly after plating (DIV 1-2). Glutamate receptors are trafficked to sites of active plasticity

(Kessels & Malinow, 2009; Malenka & Bear, 2004) so I would expect to see a detectable level of trafficking in older neurons undergoing spinogenesis both via local lateral diffusion and intracellular vesicular trafficking (Chater & Goda, 2014; Washbourne et al., 2002). Following co-treatment with competitor molecules NASPM or DNQX I would expect to see a reduction in punctate labeling due to competition for the open ion channel or glutamate binding site, respectively.

## CHAPTER 5

### RESULTS

#### Aim 1: Whole cell patch clamp electrophysiology

The goal of aim 1 was to use whole cell patch clamp electrophysiology to test the labeling of CP-AMPA receptors with nanoprobe by recording changes in glutamate-evoked current through heterologously expressed GluA1-L497Y homomultimers during, pre- and post- nanoprobe labeling.

Nanoprobe is designed to target active CP-AMPA receptors via a ligand derived from the open channel blocker NASPM. For the intrinsic ion channel of the CP-AMPA receptor to be available for interaction with NASPM, the receptor must bind an agonist to initiate opening of the ion channel (Figure 2). To evaluate nanoprobe labeling of functional, active CP-AMPA receptors we applied nanoprobe to heterologously expressed GluA1 homomultimers, both in conjunction with glutamate and without glutamate present, and measured glutamate-evoked current with whole cell patch clamp electrophysiology. We found that 1  $\mu\text{M}$  nanoprobe in conjunction with 20  $\mu\text{M}$  glutamate blocks approximately 60% of the glutamate-evoked current through active GluA1 homomultimers (n=10, Figure 7). This is in keeping with the finding by Koike et al. (1997) that 1  $\mu\text{M}$  NASPM blocked approximately 70% of agonist-evoked current, suggesting that nanoprobe ligand acts as an activity-dependent channel-blocker in a similar manner to NASPM. In contrast, following application of 1  $\mu\text{M}$  nanoprobe alone, only about 20% of glutamate-evoked current is blocked (n=6, Figure 7). This partial block may be due to residual nanoprobe in the bath. Or, over the course of the

1 minute nanoprobe incubation, stochastic channel opening may have made some ion channels available for interaction with probe ligand even in the absence of glutamate, allowing for some channels to be blocked. These results suggest that nanoprobe does indeed label active CP-AMPA receptors preferentially, supporting the supposition that nanoprobe will target CP-AMPA receptors at excitatory synapses where glutamate is being released.

Nanoprobe is also designed to be a minimally perturbing CP-AMPA receptor label, with a ligand that can be removed to relieve open-channel block of the targeted receptor after labeling. The NASPM-derived ligand is connected to the rest of the probe molecule via a photocleavable linker so that it can be cleaved with UV light after bringing the electrophilic moiety into contact with a receptor (Figure 3). Once the electrophile has covalently bound to a nucleophile on the receptor surface, the probe fluorophore will remain attached to the receptor after ligand removal. To evaluate the effectiveness of photolytic ligand release and removal of CP-AMPA receptor channel block, glutamate-induced current was probed twice with 1 second pulses of glutamate after the nanoprobe/glutamate treatment. The first glutamate pulse was delivered alone, and the second in conjunction with a 15 second exposure to 380 nm light, which relieved a significant portion of nanoprobe-induced open channel block (Figure 7). Full glutamate-response was restored after an ECS wash. This finding is consistent with the expectation that ligand is cleaved upon exposure to UV light, unblocking receptor channels and restoring normal glutamate-evoked current into the cell.

Figure 7 (Vytla et al., 2011) depicts and summarizes the electrophysiological data from HEK293T cells heterologously expressing GluA1-L497Y homomers, patched in

whole cell patch clamp configuration. Parts A and B are representative recordings from single cells treated with either glutamate and nanoprobe together (A), or nanoprobe alone (B). These recordings demonstrate the activity-dependent nature of the nanoprobe interaction with CP-AMPA receptors, and the photolytic release of ligand. In part A, one of three baseline glutamate-responses is shown, followed by 1 minute of glutamate and nanoprobe perfusion, and then 1 minute of ECS perfusion to remove any remaining nanoprobe. A 1 second pulse of glutamate was then delivered to probe the ability of the CP-AMPA receptors to open in response to glutamate. Fifteen seconds later, another 1 sec pulse of glutamate was delivered in combination with a 15 second exposure to UV light, restoring much of the glutamate-evoked current. The initial remaining partial block is likely due to residual ligand present in the bath after photocleavage, as after a 30 second ECS wash, glutamate-evoked currents were restored to normal magnitude. In contrast, cells treated with nanoprobe alone show little reduction in glutamate response even prior to application of UV light (B).

Part C summarizes and quantifies the change in peak glutamate-evoked current following treatment with either nanoprobe alone, or nanoprobe and glutamate together, before and after photolytic release of the ligand. For each treatment condition the white column represents normalized peak current in response to the first glutamate test pulse, and the purple column represents normalized peak current in response to the second glutamate test pulse, delivered in combination with UV light. For each cell, peak glutamate currents were normalized to the cell's baseline glutamate response. Prior to treatment, a baseline response to glutamate was measured using three 1 second pulses of 20  $\mu$ M glutamate, each delivered 1 minute

apart with ongoing ECS perfusion between each pulse. The average peak current for all three of these glutamate responses provides a baseline reference to which subsequent glutamate responses were normalized.

The evidence gathered from these electrophysiological experiments suggests that nanoprobe acts as a minimally perturbing label of active CP-AMPARs. Experimental results show that nanoprobe preferentially targets active, glutamate bound CP-AMPARs over inactive receptors, acting as an open channel blocker as expected. Furthermore, photolytic release of the ligand followed by ECS perfusion relieves channel block and restores normal glutamate-evoked response, indicating that the ligand is being successfully cleaved with UV light, returning the receptor to a normal gating state. Taken together, these results suggest that nanoprobe will label CP-AMPARs at glutamatergic synapses in a minimally-perturbing fashion that allows the receptor to resume normal activity after photolytic-release of ligand.

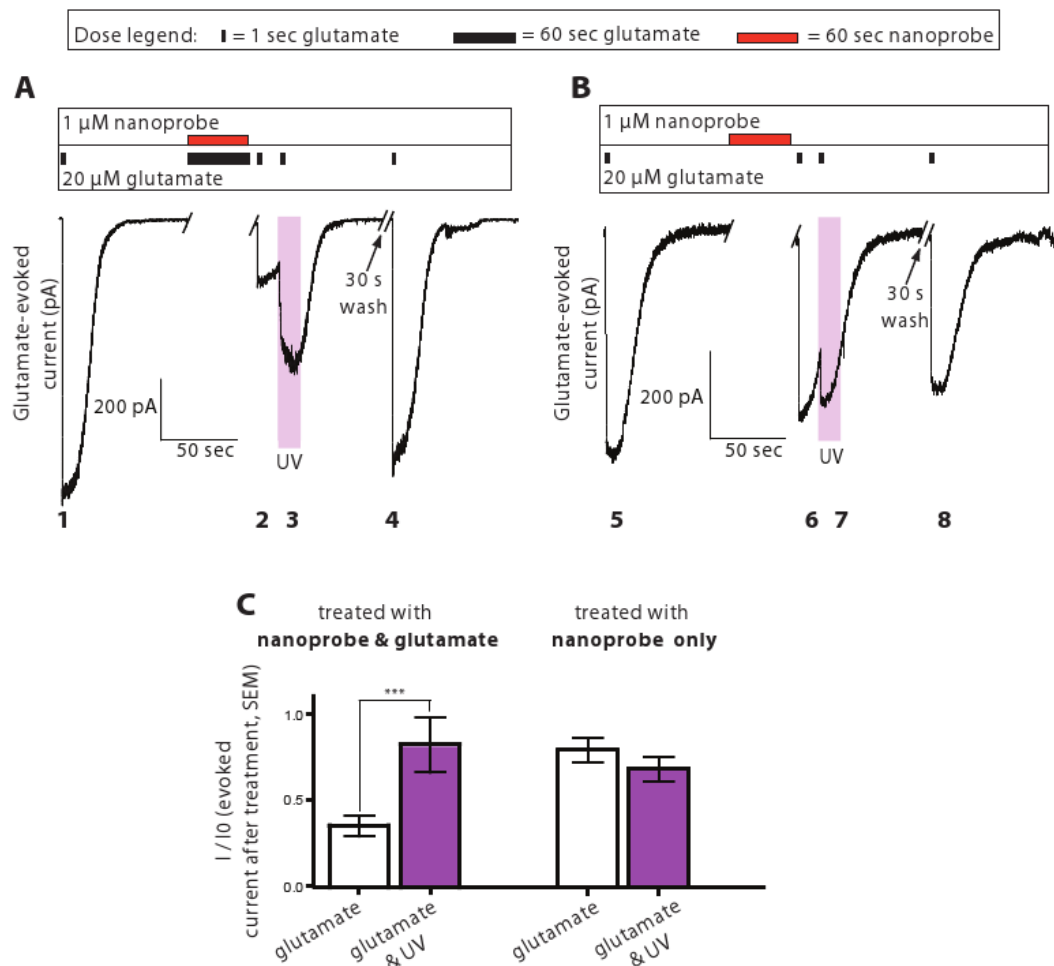


**Figure 7: Whole cell patch clamp data from HEK293T cells expressing GluA1-L497Y homomeric receptors. Nanoprobe acts as use-dependent, photocleavable blocker. A)** Representative recording from a single cell demonstrating the effect of co-application of nanoprobe and glutamate. **1.** Baseline glutamate-evoked current. **2.** Glutamate-evoked current was markedly reduced after nanoprobe/glutamate co-treatment. **3.** A portion of glutamate-evoked current was immediately restored by photolytic-release of ligand with UV light. **4.** Subsequent glutamate applications on the same cell evoked current comparable to baseline response. **B)** Representative recording from a single cell demonstrating the effect of nanoprobe application without glutamate. **5.** Baseline glutamate-evoked current. **6.** Glutamate-evoked current slightly reduced after nanoprobe treatment. **7.** Glutamate-evoked current after photolysis of the linker shows no increase. **8.** Subsequent glutamate-evoked currents reduced from baseline, indicating potential current run-down. **C)** Quantification of normalized peak glutamate-evoked current before and after photolytic-release of ligand. The two left columns represent normalized peak current before and after photolytic-release of ligand on cells co-treated with nanoprobe and glutamate ( $n = 10$ ) and the two right columns represent normalized peak current before and after photolytic-release of ligand on cells treated with nanoprobe alone ( $n = 6$ ). Data presented as mean and SEM (error bars). Photolytic-release in the nanoprobe and glutamate co-treatment group demonstrates a significantly larger glutamate-evoked current after photolytic-release ( $***P = 0.0007$ , paired t-test).

## **Aim 2: Imaging co-labeled endogenous receptors**

The goal of aim 2 was to use fluorescent imaging to evaluate nanoprobe labeling of glutamate receptors endogenously expressed in hippocampal neurons by co-labeling nanoprobe-treated neurons with traditional antibodies to AMPAR and synaptic targets.

As a first step towards visualizing nanoprobe labeling of neuronal receptors we imaged live neurons before and after nanoprobe treatments. Neuronal cultures were imaged prior to treatment, washed, incubated with nanoprobe, washed again, and re-imaged to visualize fluorescent labeling. The goal of these early labeling experiments was to determine appropriate concentrations and incubation times for nanoprobe imaging experiments. Initial results indicated that replacing the dansyl fluorophore with a different fluorescent tag might make nanoprobe labeling easier to visualize.

The initial version of nanoprobe, synthesized by Dr. Vytla Devaiah, employed dansyl as the fluorophore that would remain covalently attached to the target protein after ligand-removal. Dansyl is excited by UV light and emits maximum fluorescence intensity in the range of 500 nm. Peak emission is affected by polarity and pH (Holmes-Farley & Whitesides, 1985), making dansyl a possible candidate for reporting on the receptor environment by tracking changes in peak emission wavelength. The ligand-binding domain of AMPA receptors changes shape when transitioning from an apo to an agonist-bound state, and again to a desensitized state (Traynelis et al., 2010). Depending on the precise location of where the fluorophore was bound to a receptor surface, these conformation changes could potentially alter the pH and

polarity of the fluorophore's local environment to provide a visual signal of the receptor's current state.

Early attempts to image dansyl-nanoprobe were hampered by difficulties in detecting the fluorophore signal above high levels of background autofluorescence. Several of the primary sources of endogenous autofluorescence in cell culture are excited in the UV range and fluoresce in a broad spectrum overlapping with the dansyl emission spectrum, including NAD(P)H, flavins, and lipofuscin (Monici, 2005). This fact coupled with the low extinction coefficient of the dansyl fluorophore frequently meant that nanoprobe labeling was hidden by the overall brightness of the tissue autofluorescence in culture. We had some success using a 100  $\mu$ M concentration of nanoprobe, which produced punctate labeling along neurites when compared with background fluorescence in extracellular solution (Figure 8), though this labeling was only distinguishable in regions with few neuronal cell bodies and little to no glia present in the field of view.

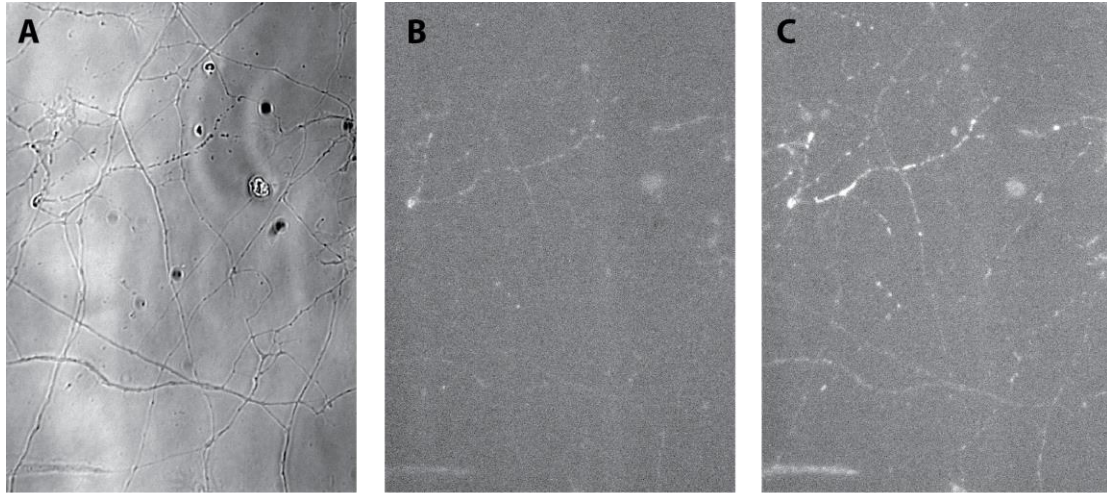


**Figure 8: Punctate staining of DIV 14 dissociated hippocampal culture treated with 100  $\mu$ M nanoprobe. A) Brightfield image. B) Background fluorescence in extracellular solution. C) Dansyl fluorescence after 5 minute incubation in 100  $\mu$ M nanoprobe, followed by 2 minute ECS perfusion. Brightness and contrast settings are identical for B and C.**

Figure 9 shows the fluorescence intensity graphed for selected regions of the neurites pictured in Figure 8 before and after treatment with nanoprobe. The fluorescence is suggestive of a pattern of labeled, spine-like puncta strung along dendrites. However, at such a high concentration of nanoprobe the likelihood of non-specific labeling increases. As previously discussed, to achieve CP-AMPA specificity the ligand portion of the probe was designed to capitalize on the pharmacology of the polyamine toxin molecules Joro spider toxin, argitoxin, philanthotoxin-433 and, most structurally similar, the synthetic CP-AMPA blocker NASPM (Brackley et al., 1993; Stromgaard et al., 1999; Stromgaard & Mellor, 2004; Yoneda et al., 2001). Each one of these molecules has been used previously to specifically target and block CP-AMPA receptors. However, some of these toxins have also been used to target CP-kainate receptors, NMDA receptors, and even to block nAChRs at high concentrations

(Bahring & Mayer, 1998; Brackley et al., 1993; Mellor et al., 2003; Ogoshi & Weiss, 2003; Stromgaard & Mellor, 2004; Sun et al., 2009; Yin et al., 2002). A more in-depth discussion of the interactions between these toxins and polyamine sensitive receptors can be found in the introduction.

Due to these potential off-target interactions it is important to use a concentration of nanoprobe within a reasonable range for targeting CP-AMPARs specifically. However, determining an accurate  $IC_{50}$  value for this pharmacological class has been the subject of some effort due to differences in reported neuronal preparation and experimental conditions. Variations in these conditions such as age of preparation, use of intact versus dissociated tissue, and concentration of agent, as well as the use-dependency and voltage-sensitivity of antagonism that these molecules exhibit have contributed to a broad range in reported efficacy. As previously mentioned,  $IC_{50}$  values from literature reports for this class of blockers range from 30 nM to 3  $\mu$ M (Brackley et al., 1993; Jackson et al., 2011). While this might make it difficult to optimize concentration, it is clear that ultimately 100  $\mu$ M is much too high of a concentration to be considered specific to CP-AMPARs, making the results of this labeling interesting but far from conclusive

To address some of these complications a new version of nanoprobe was synthesized by Dr. Devaiah, using Cy3 to replace dansyl as the fluorophore. Cy3 has a much higher extinction coefficient (Gruber et al., 2000) and an excitation maximum in the visible spectrum, at 550 nm, red-shifted away from some of the peak excitation wavelengths for the endogenous autofluorescent compounds. This change was implemented in

hopes that these more bioimaging compatible Cy3 properties would improve visibility of the fluorescent tag against the background.

After further experimentation with nanoprobe concentration, hippocampal cells were cultured, treated with 5  $\mu$ M of the new Cy3-nanoprobe, and then fixed and stained with the monoclonal anti-GluR1-NT clone RH 95 (MAB2263) antibody from Millipore, an antibody for the GluA1 subunit of AMPA receptors, targeted to the extracellular amino-terminus. GluA1 is incorporated into both calcium-permeable and non-calcium-permeable AMPARs, so we expected that most nanoprobe labeling would colocalize with GluA1, while anti-GluA1 would label many additional non-CP-AMPARs as well. Slides were imaged using confocal microscopy (Figure 10). We found punctate Cy3 labeling visible on some neurons in a pattern resembling dendritic spines, but we were surprised by the general lack of overlap between nanoprobe and antibody labeling. We hypothesized that a portion of the receptors labeled by nanoprobe had been internalized as a result of the temporary blockage of the channel pores during the 2 minute incubation with the probe. Anti-GluA1 would not have reached these internalized receptors as cell membranes were not permeabilized during antibody labeling, in which case the lack of overlap between the two tagged receptor populations could be due to one being primarily internal and one primarily external.

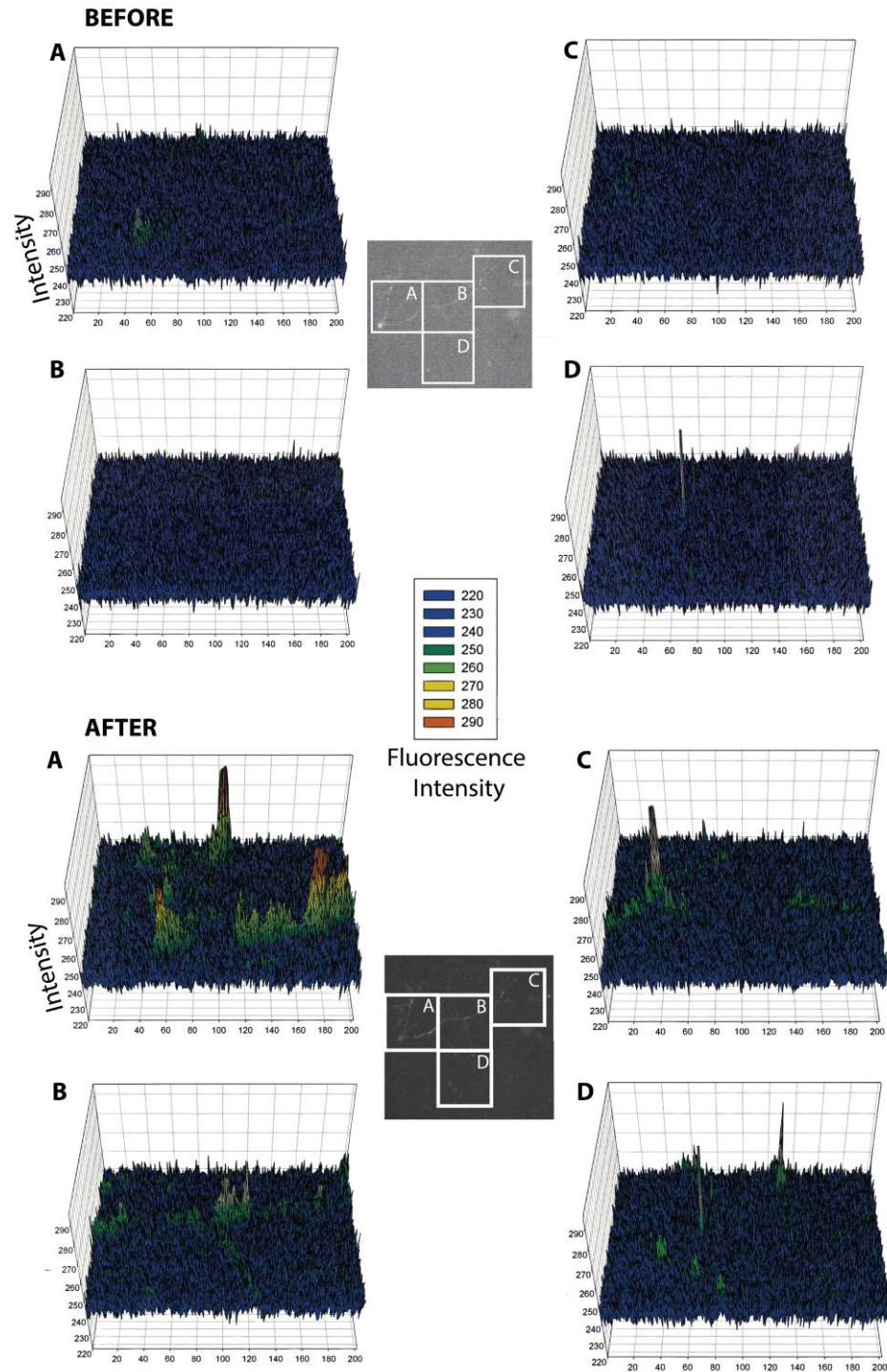


**Figure 9: Punctate patterns of fluorescence in DIV 14 dissociated hippocampal culture treated with 100  $\mu$ M nanoprobe, using neurons pictured in Figure 8. Fluorescence intensity is graphed for four selected regions of interest (A, B, C and D) before and after nanoprobe treatment. 3D mesh plots were generated in SigmaPlot.**

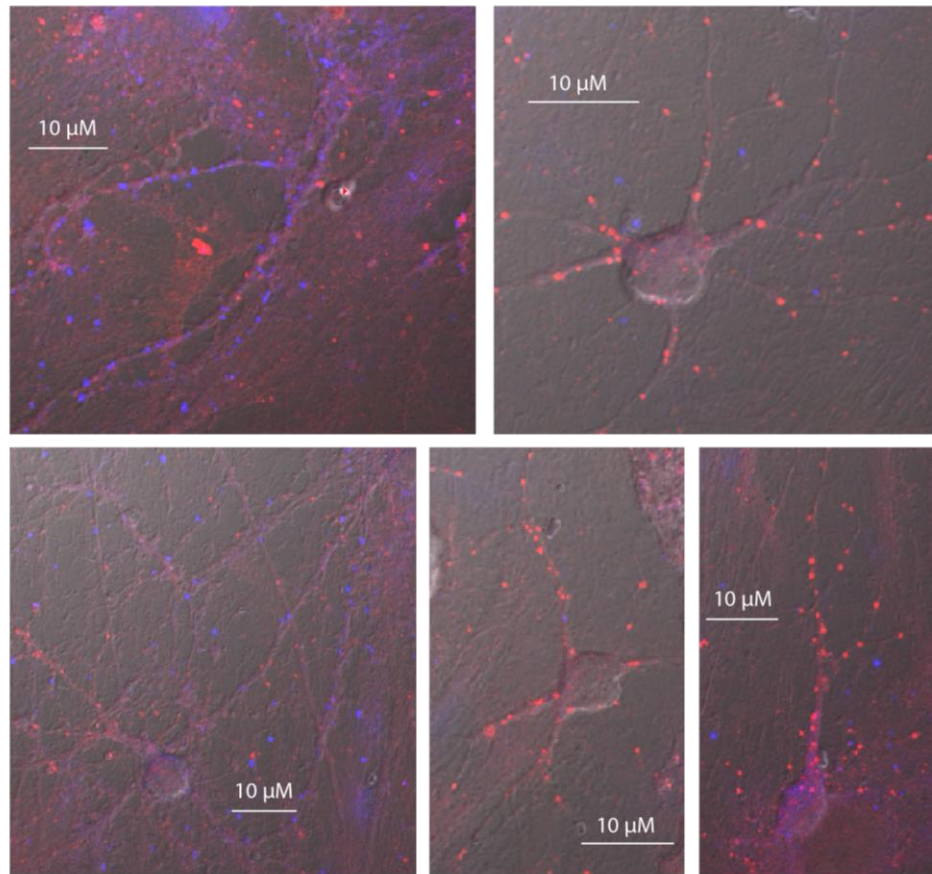


**Figure 10: DIV 24 dissociated hippocampal culture co-labeled with nanoprobe and anti-GluA1 shows little to no colocalization of the two fluorescent labels.** Coverslips were treated with 5  $\mu\text{M}$  Cy3-nanoprobe (red) for 2 minutes, fixed and labeled with anti-GluA1 using a 405 nm secondary antibody (blue). Images acquired with help from Kristina Moody in the Hebert lab.

As 5  $\mu\text{M}$  of nanoprobe is still above the 30 nM to 3  $\mu\text{M}$   $\text{IC}_{50}$  range of polyamine toxins, leaving the receptor specificity uncertain, we shifted to using lower concentrations of nanoprobe to compare probe labeling with GluA1-labeling. DIV 21 dissociated hippocampal cultures were incubated with 250 nM Cy3-nanoprobe for 2 minutes, fixed, and again labeled with the GluA1 antibody at a 1:1000 dilution. This time cell membranes were permeabilized during antibody application to allow for antibody-staining of both external and internalized receptors. The GluA1 antibody (green) was

widely clustered in puncta on somas and neurites as would be expected due to the prevalence of GluA1 subunit. In the center of some of these puncta we found smaller yellow clusters indicating potential overlap with the Cy3 label (Figures 11 and 12). We were intrigued by these results as they suggested that there could be central populations of CP-AMARs within some dendrites, however the widespread red autofluorescence in the background called into question whether these yellow clusters indicated actual receptor overlap or merely autofluorescence in the red channel. Cultures treated with higher concentrations of Cy3-nanoprobe, ranging from 500 nM to 1  $\mu$ M, fixed, and stained with anti-GluA1 primarily seemed to have an increase in red background 'speckling' making it harder to distinguish genuine labeling from background or off-target fluorescence. Increasing the concentration back up to 5  $\mu$ M also seemed to primarily increase background without improving the colocalization of nanoprobe and antibody, though cell membranes were still being permeabilized as part of the antibody staining process. Throughout this process imaging parameters were experimented with in attempts to enhance the distinction between labeled receptors and background, including exposure times, z-stack slice sizes, and averaging multiple scans together in hopes that fluorescence at receptor clusters would be more concentrated and thus persist more clearly than background fluorescence. Varying the number of washes applied pre- and post- treatment with probe did not seem to improve detection of receptors either.

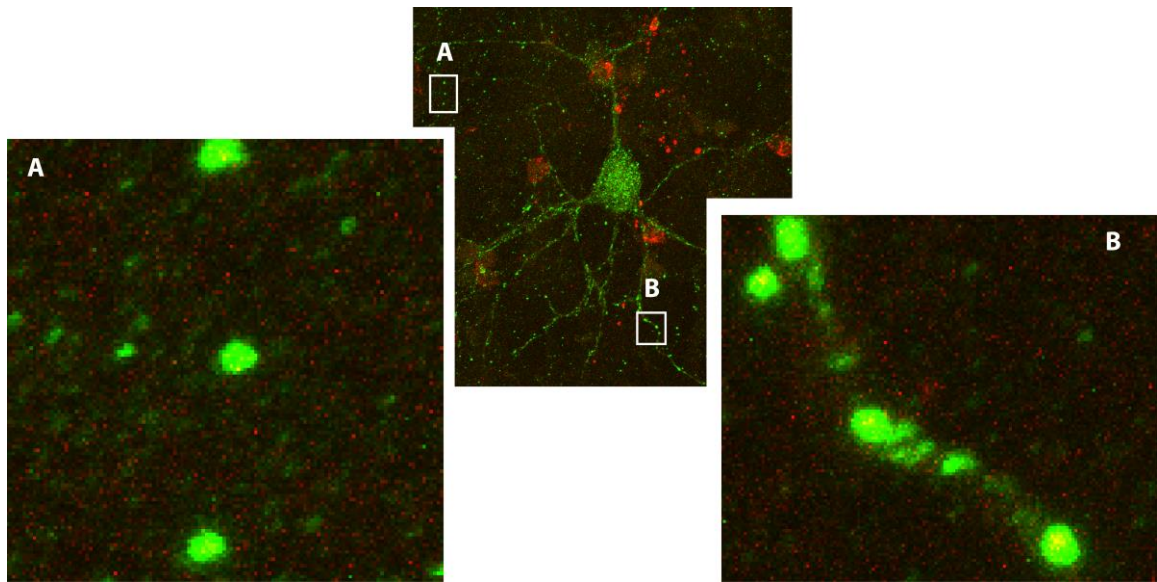


**Figure 11: Visualizing nanoprobe and anti-GluA1 colocalization.** Some GluA1-labeled puncta (green) appear to have regions of nanoprobe labeling (yellow), suggestive of CP-AMPA receptors located at synapses. DIV 21 dissociated hippocampal cultures were treated with 250 nM Cy3-nanoprobe (red) for 2 minutes, fixed, and labeled with anti-GluA1 using a 488 secondary antibody (green). Regions of overlap are yellow. Anti-GluA1 staining produced punctate labeling patterns, likely indicative of synapses. Some putative synapses had yellow regions in the center, possibly due to CP-AMPA receptors clusters in the center of the synapse. Regions **A** and **B** are magnified on the left and right, respectively, to highlight puncta of interest. Yellow areas are visible in the center of some of the anti-GluA1 clusters, indicating potential overlap between the two fluorescent labels. However, red background/autofluorescence is widespread, as can be seen in the central image.

To further elucidate probe distribution on labeled neurons, coverslips of DIV 16 to DIV 21 dissociated hippocampal culture were treated for 1-2 minutes with 250 nM, 500 nM, 750 nM or 1  $\mu$ M nanoprobe, either alone or in conjunction with 25  $\mu$ M of the AMPAR antagonist DNQX. Coverslips were then fixed and stained with anti-GluA1 antibody in hopes that comparison of these treatments would provide some clear distinction in the labeling patterns. This was not the case however. The overlap coefficient between probe fluorescence and antibody fluorescence as determined by the Zeiss LSM software ranged from 0.2 to 0.6 for treatments with nanoprobe and DNQX

combined. For coverslips treated with nanoprobe alone, overlap coefficients ranged from 0.2 to 0.7 at the upper end.

An overlap coefficient of 1 would indicate nanoprobe labeling perfectly overlapped with antibody labeling. If there were distinct differences between probe labeling of CP-AMPA treated with nanoprobe alone and CP-AMPA treated with DNQX and probe together, we would expect to consistently see an overlap coefficient closer to 1 for the nanoprobe alone condition, and a consistently smaller coefficient for the DNQX/probe combination, indicating less overlap between probe and antibody label.

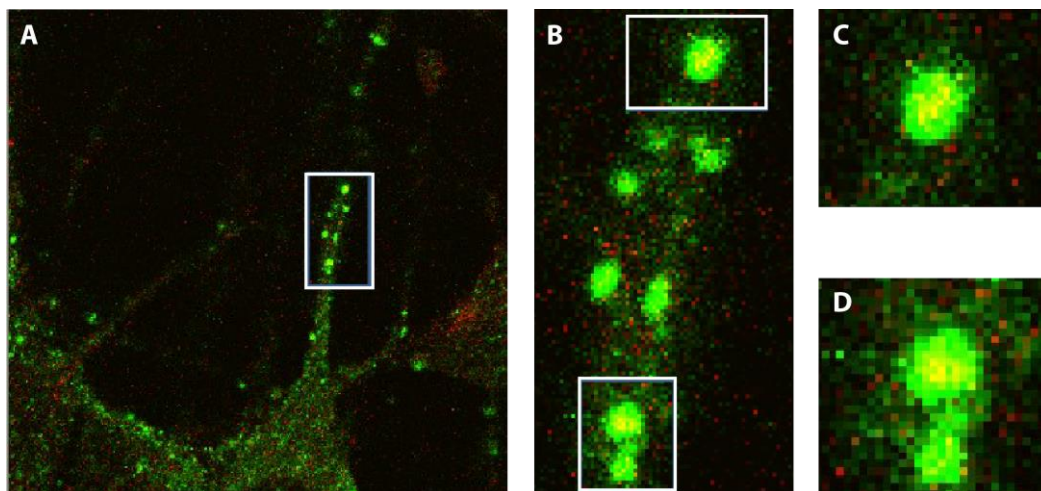


**Figure 12: Visualizing nanoprobe and anti-GluA1 colocalization.** Some GluA1-labeled puncta (green) appear to have regions of nanoprobe labeling (yellow), suggestive of CP-AMPA located at synapses. DIV 21 dissociated hippocampal cultures were treated with 250 nM Cy3-nanoprobe (red) for 2 minutes, fixed, and labeled with anti-GluA1 using a 488 secondary antibody (green). Regions of overlap are yellow. Anti-GluA1 staining produced punctate labeling patterns, likely indicative of synapses. Some of these putative synapses had yellow regions in the center, which could be due to clusters of CP-AMPA located at certain synapses. Image **A**) is a neuron labeled with nanoprobe and anti-GluA1. A neurite expressing puncta that appear to be labeled with both fluorophores is highlighted in the white box. This region is magnified in **B**) with the two puncta of interest highlighted in white boxes at the top and bottom of the image. **C**) and **D**) are magnifications of these two puncta.

Given the range of overlap coefficients for the DNQX control competition condition (0.2 to 0.6) and the range of overlap coefficients for nanoprobe alone (0.2 to 0.7), no

clear pattern seems to be emerging. Interestingly, in probe alone applications, higher nanoprobe concentrations did not correlate to higher overlap coefficients, suggesting that the lowest dose for targeting CP-AMPARs is at least equally effective as higher doses. The neuron on which the most apparent probe/antibody overlap was found was from a coverslip treated with 250 nM nanoprobe for 2 minutes. However, a closer look calls into question the significance of all of these overlap measurements. When hand-selected ROIs and background regions were compared, the difference between label overlap on a neurite of interest and label overlap on a selected region of nearby background was only  $\sim 0.1$ , indicating that overall measured overlap might be as much due to background fluorescence as colocalization on actual neuronal structures.

Initially we expected that as a majority of hippocampal AMPARs contain the GluA1 subunit (Lu et al., 2009), we should see both abundant GluA1-labeling, and nanoprobe labeled-receptors largely colocalized with the GluA1 label. However, while GluA1-labeling is abundant, we have largely failed to image this kind of colocalization.

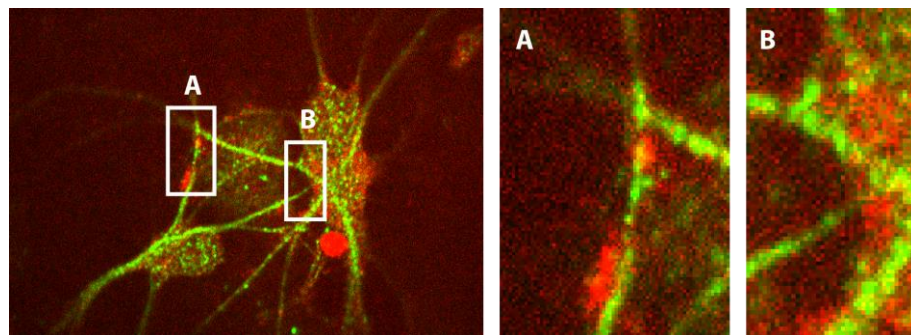


**Figure 13: Co-labeling neurons with pan-AMPAR antibody and nanoprobe does not result in clear probe labeling of receptors.** DIV 24 Dissociated hippocampal culture treated with 300 nM nanoprobe (red) for 1-2 minutes, fixed and labeled with pan-AMPAR antibody from Santa Cruz Biotech (GluR 1/2/3/4 H-180, SC-33612) at 1:200 dilution, using a permeabilizing blocking buffer, treated with a 488 secondary antibody (green). Regions **A**) and **B**) are magnified to increase detail.

Perhaps the placement of the nanoprobe itself on the receptors interferes with the antibody recognition of its target by disrupting binding interactions with a key residue (Janeway et al., 2001), or perhaps under our culture conditions the number of CP-AMPARs expressed is too small to be readily visible above background. As a point of comparison we also co-treated neurons with nanoprobe and a polyclonal pan-AMPAR antibody for labeling all AMPA receptors. An example is shown in Figure 13. However, these experiments also failed to reveal clear receptor labeling, with background fluorescence seeming to be brighter than any synaptic or receptor labeling. Out of all of these attempts using anti-GluA1 and pan-AMPAR antibody to demonstrate co-labeling of receptors, while colocalization between nanoprobe and antibody seemed minimal, when we did manage to image what appeared to be true nanoprobe labeling of receptors on neurites at levels well above background fluorescence, the pattern of fluorescence was punctate along neurites and soma as would be expected if labeling dendrites (Figure 10).

To colocalize nanoprobe with an antibody targeted to something other than AMPARS themselves, and to visualize the proximity of nanoprobe-labeled receptors to synapses, we treated neurons with probe and then stained them with an antibody for a pre-synaptic protein. DIV 23 neurons were treated with 200 nM nanoprobe for 1, 2 or 5 minutes, either alone or in conjunction with 20  $\mu$ M glutamate, fixed, and stained for the pre-synaptic protein synapsin-1 using a 488 secondary antibody. The Cell Signaling synapsin-1 (D12G5) XP #5297 monoclonal antibody was used at a 1:500 dilution, with a permeabilizing blocking buffer. Coverslips were imaged using a spinning disk confocal microscope. By treating cultures for a variety of times, we

hoped to gain a clearer picture of whether receptors were being internalized after a certain period of time incubating with nanoprobe.

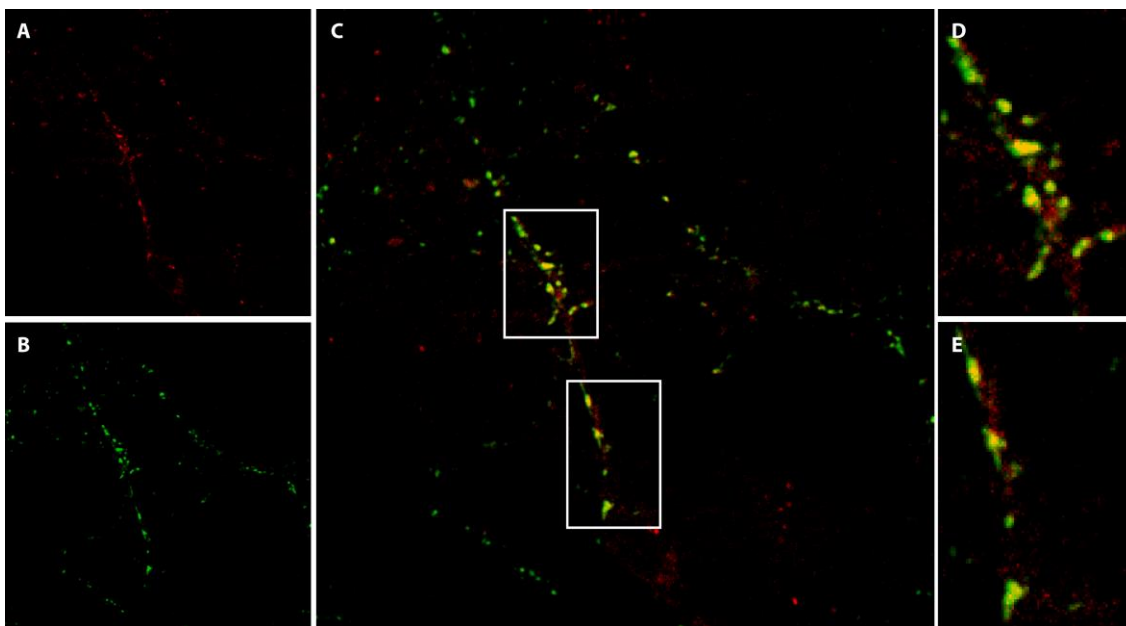


**Figure 14: Nanoprobe fluorescent labeling (red) colocalized with anti-synapsin-1 Cell Signaling antibody (green).** DIV 23 dissociated hippocampal neurons treated with 200 nM nanoprobe and 20  $\mu$ M glutamate for 2 minutes, fixed, and labeled with anti-synapsin 1. **A)** Nanoprobe labeling in red. **B)** Anti-synapsin staining in green. **C)** Composite image of nanoprobe and anti-synapsin labeling, yellow regions indicate areas of overlap. **E)** and **D)** are magnifications of the areas in white boxes in **C)**. The relatively large amount of apparent colocalization is unusual for nanoprobe fixed cell imaging. Out of 25 regions from 8 different coverslips encompassing several nanoprobe treatment regimens, this was the only cell demonstrating notable overlap between nanoprobe and antibody labeling.

After selecting images that appeared to have the most distinct nanoprobe labeling, 5 fields of view treated with nanoprobe alone and 4 treated with glutamate and nanoprobe together were analyzed for colocalization. Sites of synapsin staining were identified and used to determine ROIs, then analyzed for overlap with nanoprobe labeling. On coverslips treated with nanoprobe alone, out of 1207 synapsin-stained ROIs we found 46 (3.81%) that were also labeled with nanoprobe. For coverslips treated with both glutamate and nanoprobe, 659 ROIs were identified, out of which

59 (8.95%) were co-labeled with nanoprobe. As indicated by the low colocalization values most neurons in both treatment conditions had very little overlap of synapsin and nanoprobe staining (Figure 15), though one notable neuron had nearly fifty percent colocalization (Figure 14). After both treatment conditions the overall nanoprobe staining intensity was typically low compared to background intensity, with the exception of the neuron that showed such extensive colocalization. Finding an example of punctate nanoprobe labeling with a high percentage of overlap with synapsin-1 labeling could suggest that the apparent overall low level nanoprobe labeling found in our fixed cells is due to a general lack of CP-AMPA expressing neurons in our DIV 20-23 dissociated cultures.

As a point of comparison, untreated neurons were washed with ECS, fixed and imaged using the same acquisition settings as those used for coverslips co-labeled with nanoprobe and synapsin (Figure 16). Brightness settings were adjusted to be the same as those used to visualize probe labeling in Figures 14 and 15, and though these neurons were untreated with nanoprobe, they displayed comparable levels of red fluorescence to nanoprobe-treated neurons. Given these results it seems that red autofluorescence in the fixed cells may frequently be obscuring nanoprobe labeling.

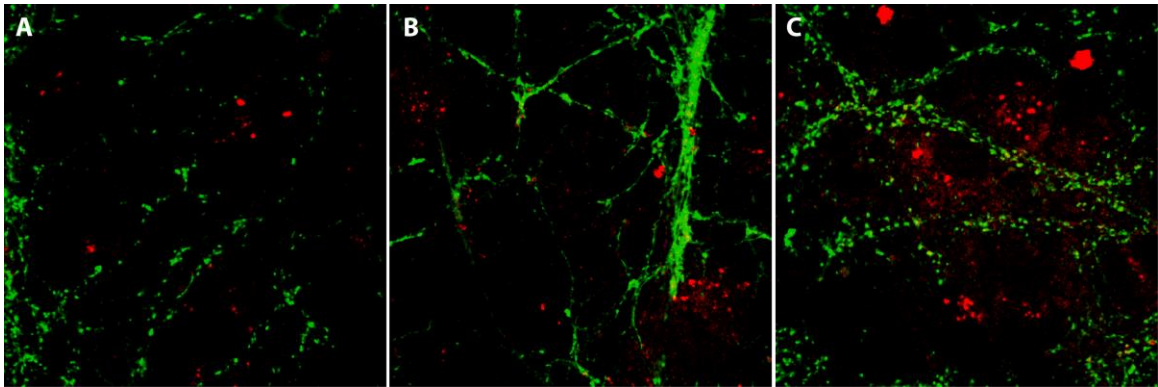


**Figure 15: Nanoprobe fluorescent labeling (red) rarely colocalizes with anti-synapsin-1 Cell Signaling antibody (green).** Representative images of DIV 23 dissociated hippocampal neurons treated with 200 nM nanoprobe in conjunction with 20  $\mu$ M glutamate or 20  $\mu$ M NASPM, fixed, and labeled with anti-synapsin-1. **A)** Neurons treated with 200 nM nanoprobe and 20  $\mu$ M glutamate for 2 minutes, labeled with anti-synapsin-1. **B)** Neurons treated with 200 nM nanoprobe and 20  $\mu$ M glutamate for 5 minutes, labeled with anti-synapsin-1. **C)** Neurons treated with 200 nM nanoprobe and 20  $\mu$ M NASPM for 5 minutes, labeled with anti-synapsin-1. Treatment with nanoprobe and glutamate in combination typically produced little overlap in nanoprobe and synapsin labeling. Treatment with nanoprobe and the open-channel blocker NASPM produced similar lack of colocalization. All brightness and contrast settings are identical within the group and with Figure 14.

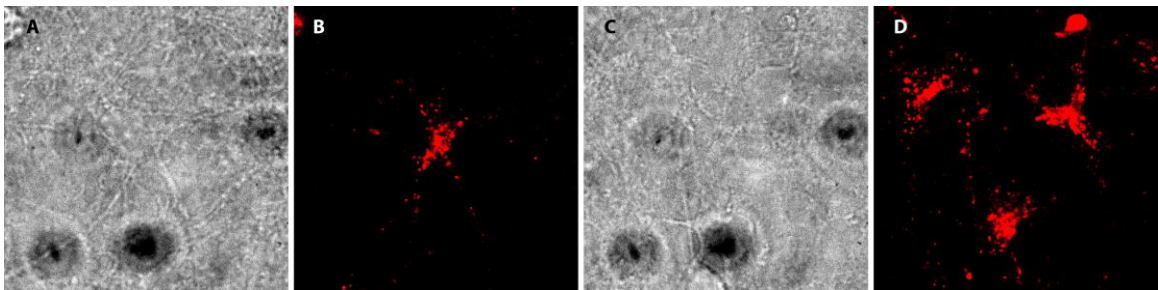


**Figure 16: Images of untreated neurons express significant autofluorescence in the red channel.** **B)** and **D)** are Images of DIV 23 dissociated hippocampal neurons obtained and presented using the same acquisition and brightness settings as used for images in Figures 14 and 15. **A)** and **C)** are the accompanying brightfield images.

Ongoing attempts to visualize nanoprobe labeling on fixed dissociated neuronal cultures has produced little in the way of clear, consistent punctate labeling. To visualize nanoprobe staining on fixed cells without antibody present, DIV 22 cultures were labeled with 30 nM, 100 nM, 300 nM, and 3  $\mu$ M of nanoprobe for incubation

periods of 10 seconds, 1 minute and 10 minutes to evaluate the effectiveness of nanoprobe at different concentrations and for different periods of labeling. Five regions on each coverslip were randomly selected and imaged using the 561 laser of a spinning disk confocal microscope, 40 slices per image separated by 0.2  $\mu\text{m}$  increments. While the highest concentration of nanoprobe showed a stronger overall fluorescence intensity, no combination of treatments consistently generated any kind of labeling that could clearly be distinguished as separate from background/autofluorescence. Representative images from coverslips treated for 1 minute with varying probe concentrations can be seen in Figure 17

As a follow-up, DIV 19 dissociated neurons were labeled with 30 nM, 100 nM, 300 nM, and 3  $\mu\text{M}$  nanoprobe either in combination with 20  $\mu\text{M}$  glutamate or with nanoprobe alone for incubation periods of 10 seconds, 1 minute and 10 minutes to determine if the inclusion of glutamate would establish clearer labeling patterns. Again, 5 regions on each coverslip were selected, this time using the bright-field view to locate clearly visible, healthy-looking neurons. Coverslips were again imaged using the 561 laser of a spinning disk confocal microscope (Figure 18). Red fluorescence appeared to be more concentrated in clusters within cells in a manner consistent with receptor internalization, as compared to the often more diffuse red fluorescence seen in cells treated with nanoprobe alone. AMPAR endocytosis can increase in response to glutamate application (Carroll et al., 2001; Lissin et al., 1999) so this pattern could be

attributable to nanoprobe-labeled receptors being internalized when co-treated with glutamate.

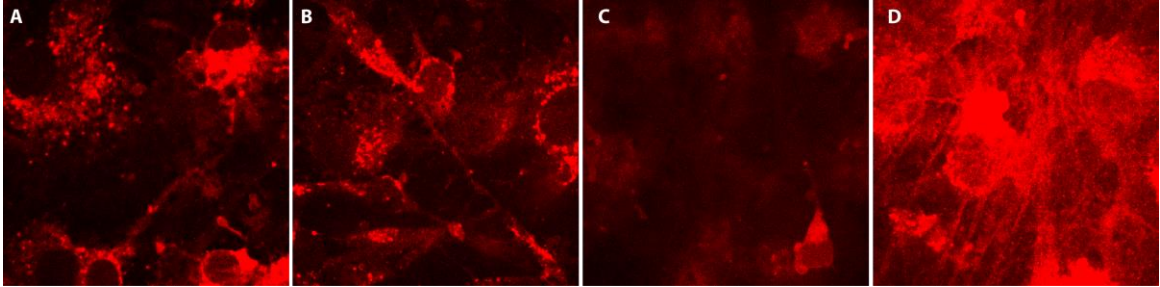


**Figure 17: Images of randomly selected regions of coverslips treated with nanoprobe for varying times at varying concentrations failed to reveal any clear probe labeling in punctate patterns above background fluorescence.** Representative images chosen for clearest labeling of apparent neuronal structures. DIV 22 dissociated neurons treated with varying concentrations of nanoprobe for 1 minute and fixed. Coverslips treated with **A)** 30 nM nanoprobe, **B)** 100 nM nanoprobe, **C)** 300 nM nanoprobe, **D)** 3  $\mu$ M nanoprobe. The 3  $\mu$ M treatment consistently showed an overall increase of fluorescence throughout the tissue in the 561 channel. All brightness and contrast settings are identical.

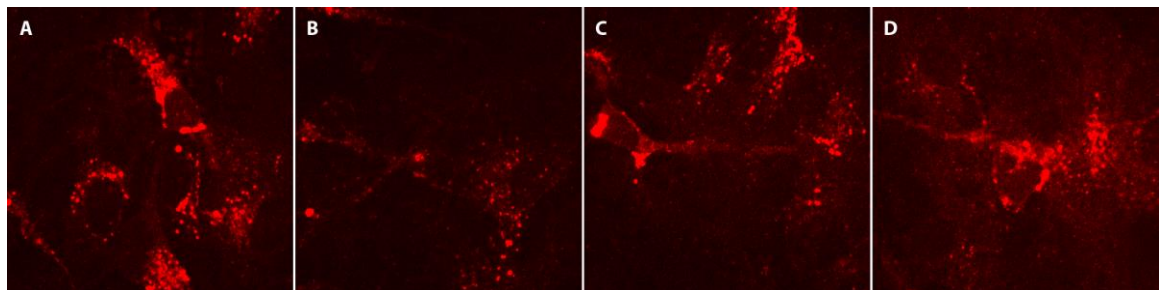


**Figure 18: Coverslips treated for varying times with glutamate and with varying nanoprobe concentrations did not reveal any clear probe labeling in punctate patterns, though increased clustering of objects fluorescing in the red channel was seen.** Representative images chosen for clearest labeling of apparent neuronal structures. DIV 19 dissociated neurons treated with 20  $\mu$ M glutamate and varying concentrations of nanoprobe for 1 minute, and fixed. Coverslips treated with **A)** 30 nM nanoprobe, **B)** 100 nM nanoprobe, **C)** 300 nM nanoprobe, **D)** 3  $\mu$ M nanoprobe. All brightness and contrast settings are identical.

After extensive attempts to image nanoprobe colocalization with fluorescent antibodies to AMPAR and synaptic targets, it was rare to find clear examples of receptors or synapses co-labeled with both nanoprobe and antibody. The original dansyl fluorophore was replaced with Cy3 to reduce autofluorescence. Nanoprobe concentrations and incubation periods were varied to reduce possible off-target interactions and to avoid potential receptor internalization, and during antibody application membranes were permeabilized to allow antibody access to endocytosed receptors. Even given these variations, there appeared to be little overlap between nanoprobe and antibody labeling, apart for one very notable exception (Figure 14), and possibly Figures 11 and 12. Occasionally there were examples of what appeared to be punctate nanoprobe labeling that did not overlap with antibody labeling (Figure 10). However, when untreated neurons were fixed, imaged, and visualized using the same parameters as those used for imaging and visualizing nanoprobe-labeling, significant red autofluorescence was present (Figure 16). Taken all together these results suggest that we may be capturing some true nanoprobe-labeling, but that autofluorescence may be masking too much of it for the images to be useful. Or perhaps low CP-AMPA expression has made it difficult to locate true examples of nanoprobe-labeling. Perhaps off-target labeling has led to red fluorescence where there should be none, though given the significant amount of red autofluorescence present in totally untreated neurons, off-target labeling is not required to explain extensive background/autofluorescence.

Overall it seems that co-labeling endogenous glutamate receptors on dissociated neurons with nanoprobe and fluorescent antibodies targeted to AMPAR and synaptic

targets has offered few successful examples of clear co-labeling, with a few interesting exceptions or partial exceptions. From these results it remains unclear if nanoprobe is largely being obscured by autofluorescence, if CP-AMPA expression is just really low, if nanoprobe is having more off-target interactions than expected, or some combination of these three explanations. It does seem that studying fixed and labeled cells is an ineffective way to research nanoprobe labeling patterns.

### **Aim 3: Imaging and tracking nanoprobe-labeled receptors** **on live neurons**

The goal of aim 3 was to use nanoprobe to detect endogenously expressed CP-AMPA receptors during the course of neuron development. Live neuronal cultures will be imaged before and after nanoprobe labeling in young dissociated cultures (DIV 1-2) and in maturing cultures (DIV 14-17).

In live, maturing neuronal cultures (DIV 14-17) we have found that nanoprobe application produces abundant fluorescent labeling at putative synaptic spines, and that these labeled sites can be observed to undergo local trafficking as well as active intracellular transport during the course of minutes, in a manner consistent with receptor trafficking. In experiments using younger cultures (DIV 1-2) we have visualized labeling of elaborate networks of tubular vesicles which traffic along neurites and rapidly move in and out of the soma. Control competition experiments demonstrate that the labeled proteins are likely CP-AMPA receptors, as the majority of

labeling is blocked by either competition with NASPM or DNQX in both young and mature cultures.

### **Dose-dependent labeling of live neurons with nanoprobe**

To determine a useful concentration range for labeling live neurons with nanoprobe, coverslips of live DIV 14-17 neurons were washed 3 times with extracellular buffer, imaged to establish background fluorescence, and then treated with 100 nM nanoprobe in extracellular buffer for 5 minutes. After this incubation period with a low concentration of nanoprobe, the coverslips were gently washed 3 times with extracellular buffer and imaged again. Finally, the same region of the coverslip was used to assay a higher concentration of nanoprobe, independently either 300 nM, 1  $\mu$ M, or 3  $\mu$ M in extracellular buffer. A 5 minute incubation in the higher concentration of nanoprobe was followed by 3 washes with extracellular buffer prior to resuming imaging (Figure 19). We performed this treatment and imaging regimen so that we could compare labeling within a range of concentrations similar to the IC<sub>50</sub> reports for the pharmacological class on which nanoprobe is based (Brackley et al., 1993; Jackson et al., 2011).

Nanoprobe concentrations of 100 nM were not statistically different from background fluorescence on any of the neurons we tested. However, 300 nM nanoprobe resulted in an increase in fluorescence, with accumulations of peak brightness on neurites in a punctate pattern that typically appeared to be located at synaptic spines as judged by bright-field morphology. Use of nanoprobe concentrations of 1  $\mu$ M or 3  $\mu$ M demonstrated a marked increase in accumulated fluorescence, however some of this

labeling appeared to be non-specific in nature, particularly at 3  $\mu$ M. As a 5 minute incubation of 300 nM nanoprobe sufficed for robust labeling (Figure 19) of punctate areas on neurites, treatments of 300 nM nanoprobe were used for subsequent labeling of live neuronal cultures.

### **Nanoprobe labeling of live neurons is prevented by co-incubation with competitor molecules**

To test nanoprobe specificity for CP-AMPA receptors under live imaging conditions, probe was applied to DIV 14-17 neuronal cultures in conjunction with non-fluorescent competitor molecules. Use of live neurons allowed us to image nanoprobe labeling of the same neurons under competition conditions and when treated with nanoprobe alone. Each coverslip was washed 3 times and imaged to establish background fluorescence before application of any treatments. Coverslips were then co-treated with nanoprobe and the competitor molecule, washed thoroughly with ECS, imaged, treated with nanoprobe alone, and washed and imaged again. NASPM and DNQX were separately

evaluated as competitor molecules to nanoprobe, with reduced fluorescent nanoprobe labeling as an indicator of effective competition.

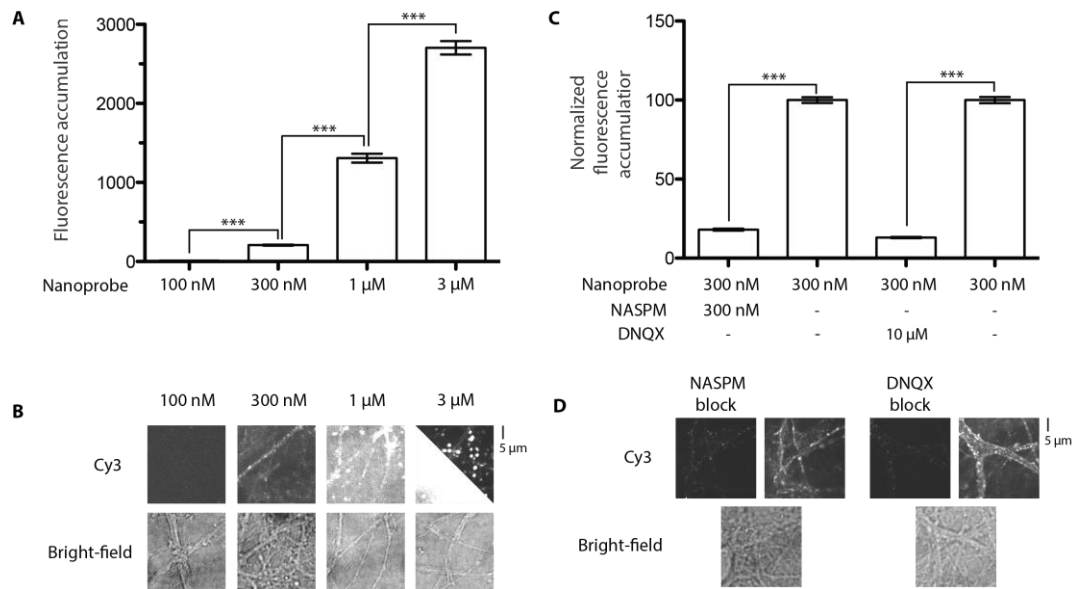


**Figure 19: Nanoprobe labels DIV 14–17 neurons in a concentration-dependent manner and can be blocked by competitive antagonists. A)** Fluorescence accumulation at puncta increases with increasing concentration of probe. Bar graph represents background subtracted group data [9 coverslips for 100 nM (4664 puncta) that were subsequently used for collecting data on 300 nM (1955 puncta), 1  $\mu$ M (1166 puncta), and 3  $\mu$ M (1543 puncta), error bars represent 95% confidence intervals,  $***p < 0.0001$ , one-way ANOVA, Dunn's multiple-comparison test]. **B)** Representative paired fluorescence and bright-field images from (A). All brightness and contrast settings are identical with the exception of the top, right half of the 3  $\mu$ M fluorescence image, which is set to show contrast at this high concentration. **C)** Fluorescence accumulation can be prevented with co-incubation. Either 300 nM NASPM or 10  $\mu$ M DNQX can significantly prevent 300 nM nanoprobe labeling of cells. Bar graph represents background subtracted data that were normalized to peak fluorescence intensity collected 1 min after washing away non-bound nanoprobe alone (3 coverslips for each condition [1766 puncta for NASPM experiment, 2021 puncta for DNQX experiment], error bars represent 95% confidence intervals,  $***p < 0.0001$ , one-way ANOVA, Dunn's multiple-comparison test). **D)** Representative paired fluorescence and bright-field images from (C). All brightness and contrast settings are identical.

Co-incubation with a stoichiometric concentration of NASPM was used to determine if the probe molecule was reacting with off-target proteins or if it was targeting the same ion conduction pore site as NASPM. We hypothesized that NASPM co-incubation should block some, but not all, of our probe labeling since the two molecules

share the acylated polyamine ligand. Co-incubation of neuronal cultures with a combination of 300 nM nanoprobe and 300 nM NASPM resulted in a modest increase in fluorescence intensity (18.1% increase) when compared to background fluorescence (Figure 19, C). When these same fields of view were treated with 300 nM nanoprobe alone, a large increase in fluorescence was observed, indicating that NASPM is indeed competing with nanoprobe for binding sites. This peak fluorescence generated by nanoprobe treatment alone provided the maximal, normalized fluorescence in this experiment, 100%. Since NASPM is a non-covalent binder, we expected this stoichiometric competition experiment to result in at least 50% labeling of binding sites because nanoprobe should kinetically trap the binding event. NASPM is a non-covalent drug whereas nanoprobe forms a covalent bond with no off-rate and thus acts as a kinetic trap until photolysis of the nitroindoline releases the ligand. The fact that NASPM blocks the majority of the fluorescence accumulation of nanoprobe labeling suggests that the binding affinity of NASPM is significantly higher than that of nanoprobe. Though the affinity of NASPM for target proteins was higher than expected in comparison to nanoprobe, this result still provides evidence that NASPM and nanoprobe do compete for the same binding sites as expected (Figure 19, C and D).

To assay the specificity of nanoprobe for AMPA receptors we performed another competition experiment, this time with DNQX, a competitive antagonist for the glutamate-binding site. Similar to the previously described experiment, after the nanoprobe/DNQX co-treatment, coverslips were washed and treated with 300 nM nanoprobe alone. The nanoprobe ligand is designed to interact with the intrinsic ion

channel conduction pore of CP-AMPARs when the channel is activated. DNQX blocks the glutamate-binding site of AMPARs and kainate receptors, and is expected to prevent channel opening. Thus, we expected co-incubation with 10  $\mu$ M DNQX to prevent fluorescent labeling with 300 nM nanoprobe. Indeed, when we co-treated DIV 14–17 neurons with a combination of DNQX and nanoprobe, we found a slight increase in fluorescence intensity (13.1% increase) when compared to background fluorescence (Figure 19, C.). When we co-treated these same fields of view with 300 nM nanoprobe alone, we observed a large increase in fluorescence. Again, this peak fluorescence provided the maximal, normalized fluorescence in this experiment, 100%. This marked increase in fluorescence intensity suggests that nanoprobe labeling is dependent on probe specificity for glutamate receptors that are sensitive to DNQX antagonism. The DNQX data combined with the block of fluorescence accumulation demonstrated by co-treatment with NASPM suggest that the target of nanoprobe labeling is indeed NASPM-sensitive glutamate receptors, very likely CP-AMPARs.

Images were analyzed using ImageJ (U.S. National Institutes of Health, Bethesda, MD, USA) (Schneider et al., 2012). To allow for quantification of nanoprobe accumulation, regions in the field of view which demonstrated fluorescence after nanoprobe application (which occurs either after low dose or after pharmacological competition experiment) were identified by applying the Triangle threshold, a method to geometrically find the maximal data within the largest histogram range (Zack et al., 1977). These thresholded images were used as input for particle detection to generate an exhaustive ROI (region of interest) list of all labeled

regions in the field of view. These ROIs were then applied to the previous time points for quantification of fluorescence during either low dose or competition incubations. Fluorescence intensities were quantified using the mean gray value of regions labeled with nanoprobe. Fluorescence intensity was then measured at these same regions for all previous and following time points. To correct for background fluorescence, three background ROIs were drawn where there was an absence of visible cells in the corresponding bright-field image. The mean intensity of these areas was used to calculate the average background that was then subtracted from the mean gray value of ROIs at each time point to determine background fluorescence before treatment, fluorescence after treatment with control (competition or low dose) solution, and fluorescence after treatment with nanoprobe alone. All brightness and contrast settings are equal within groups for comparative images presented in Figure 19 except in the one case where indicated. Group mean values at each concentration (Figure 19, A) or treatment condition (Figure 19, C) were compared to the respective control values using a one-way non-parametric Kruskal–Wallis test (Mangiavacchi & Wolf, 2004). The significant differences were further analyzed with Dunn's multiple comparison test. In all cases,  $p < 0.05$  was considered statistically significant and individual  $p$  values are provided for each test. Asterisks in the figure represent statistically significant differences. The values on the graph are expressed as means  $\pm$  95% confidence interval unless otherwise noted.

## **Tracked movements of nanoprobe-labeled receptors: DIV 14-17**

To visualize receptor labeling and trafficking in neuronal cultures, live cells (DIV 14–17) were washed with extracellular buffer and incubated with 300 nM nanoprobe for 5 min in the dark, exposed to 405 nm light for photolysis of the nitroindoline, washed again, and imaged to compile a time-series. We found numerous examples of both stable spots of fluorescence and of receptor clusters that moved either locally or comparatively long distances along a neurite and, at times, across the entire field of view (Movie S1 is demonstrative of these diverse movements and Movie S2 is a sub-region of Movie S1 that contains colored lines to demonstrate the detected movements). The relatively fast moving clusters of receptors traveling along neurites appear to be intracellular and in vesicular packages undergoing active transport based on their common movement paths. The velocities of the clustered movements that we observed are consistent with intracellular vesicular transport observed in normal neurons (Turina et al., 2011). Vesicular packages of AMPA receptors have been reported elsewhere, and the movements we observe here closely resemble the trafficking that others have observed for fluorescently-tagged glutamate receptor subunits in vesicles (Ju et al., 2004; Washbourne et al., 2002).

Tracking data from experiments with DIV 14–17 neurons (Figure 20) was generated with Matlab using a custom-built particle tracking software package (Pelletier et al., 2009). To detect the spots that were moving rapidly along neurites as well as those that were relatively stationary, we used a feature size of three pixels. Each image in the time series was initially filtered to suppress high frequency noise and low frequency background variations. The time series images were collected as a series of

single z-plane images and thus, particles that move out of focus or into focus during the acquisition are either lost midway through tracking or commenced midway through tracking (Movie S2 demonstrates the effect of tracks being lost and started at different time points). The filtered image was then processed to find local intensity maxima, which are then used as estimated positions in integer pixels for the features sought. To refine the feature position about each local maximum, an area surrounding the estimated position of radius three pixels was extracted from the image, and the refined centroid position was used as the center for a second iteration of area extraction and centroid determination. This process yielded the final, calculated center position in two dimensions with a computed accuracy of 7 nm. To reliably find features in the face of photobleaching and consequent signal-to-noise degradation, the criteria for minimum integrated signal intensity and average signal intensity for each feature were adjusted automatically throughout the time series, following initial careful determination of appropriate acceptance criteria. We manually inspected the tracked particles toward the end of each time series to be certain we were robustly tracking particles that were easily visible. These criteria were then linearly adjusted to the initial frames of the time series so that particles with similar properties could be tracked in both early and late frames of each time series. Tracking in time can help discriminate noise from real features, as noise will typically not be spatially and temporally coherent. To define tracks and movements, the features that were found were allowed to move a maximum of eight pixels between frames and were required to be tracked for a minimum of 15 frames. The tracks were then overlaid onto the original time-lapse series and manually checked to confirm their acceptance as bona fide tracks.

We found that the labeled receptors in vesicles move at a fairly wide range of mean velocities (Figure 20) with two groups appearing from the particle tracking analysis. Some of these clusters move very quickly along tracks defined by neurites while others remain stationary, appearing to undergo thermal or non-active motion during imaging. After quantifying the mean velocity of 930 moving particles from five independent time-lapse experiments, we found that the mean end-to-end velocity of these clusters is 31.25 nm/s and a mean instantaneous velocity of 132.4 nm/s. The end-to-end velocity is a measure of overall movement where the instantaneous velocity provides information on the full range of velocity experienced by individual particles.

The observed movements of labeled receptors are consistent with the previously reported velocities for trafficking of GluA1 and GluA2 receptor subunits. Our results quite closely match previous reports in which fluorescent fusion protein subunits were tracked in dissociated cortical cultures at DIV 3–4 (Washbourne et al., 2002) and GluA1 and GluA2 subunits tagged with FAsH or ReAsh were tracked in dissociated hippocampal cultures at DIV 8–9 (Ju et al., 2004). As mentioned above, after labeling with nanoprobe, we found an average end-to-end velocity of about 31 nm/s, which is almost identical to the velocity that Washbourne et al. (2002) observed for GluA1 clusters uncombined with NR1, and to the velocity that Ju et al. (2004) observed for GluA1 and GluA2 clusters. Thus, our observations of very similar intracellular

trafficking velocities suggest that our labeling methodology is comparable to more complex genetically engineered methods used for observing receptor movement.

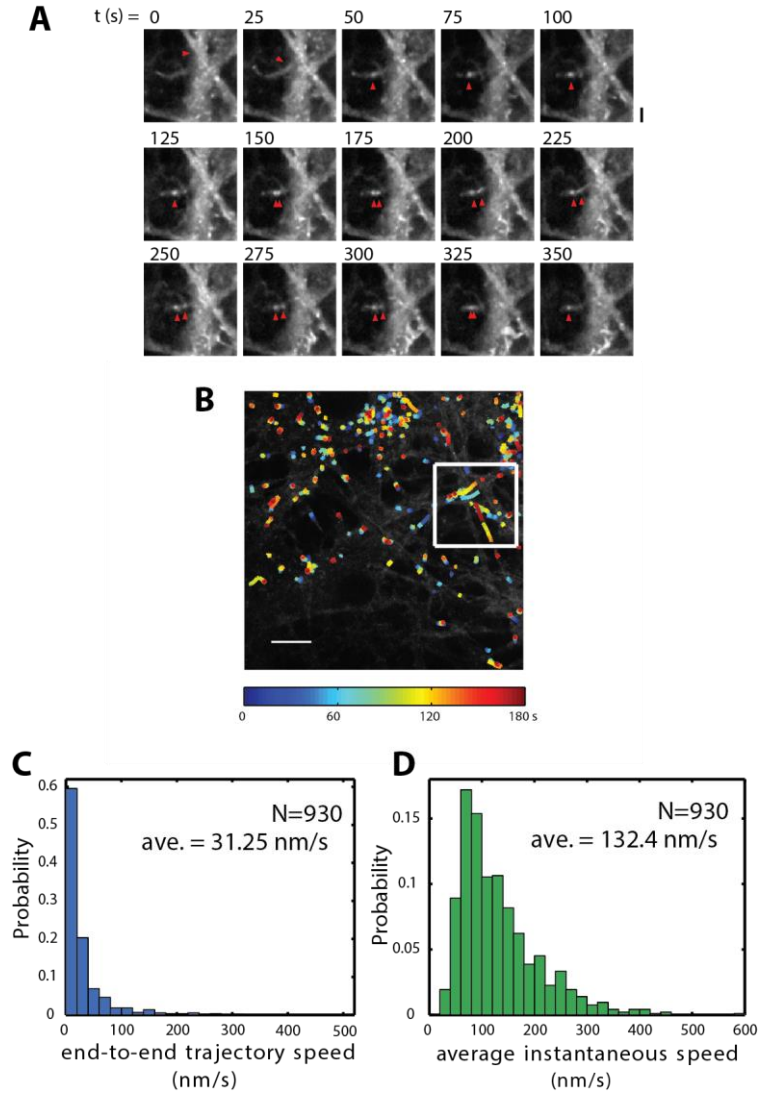


**Figure 20: Movements of nanoprobe-labeled receptors.** (A) Example of a moving cluster indicated by red arrowheads that is delivered to a putative synaptic spine. Time = 0 when the receptor cluster became visible. Scale bar for images is  $2\ \mu\text{m}$  long. (B) Overlay of detected trajectories of a number of particles moving along neurites. Colors of tracks indicate time of detection (blue = 0 s, red = 180 s). Scale bar for image is  $10\ \mu\text{m}$  long. White box corresponds to Movie S2 in which clusters are highlighted and tracked. (C) Binned histogram of end-to-end trajectory speed of 930 mobile clusters from five separate time-lapse sequences. (D) Binned histogram of instantaneous speed of 930 mobile clusters from five separate time-lapse sequences.

In addition to the movement of vesicular-located receptors along neurites, we also observed receptors in vesicles being delivered to a putative synaptic spine (Figure 20, A and Movie S3). We believe that these labeled receptors were expressed on the surface where they were labeled with our probe prior to endocytosis during the 5 min incubation period and then recycled. Because the probe does not cross the membrane unassisted, we can surmise that these fluorophores are appended to previously exposed CP-AMPARs.

In addition to intracellular movements of labeled receptors, we have also observed that areas of strong nanoprobe labeling can be found to migrate locally in response to excitatory stimuli. In some cases, during global bath application of glutamate to nanoprobe-labeled neurons, we observed the movement of labeled receptors into putative synaptic spines (Figure 21, A and B). It would be interesting to carry out further study of this effect in acute slices where synapse organization is more predictable than that found in dissociated culture.

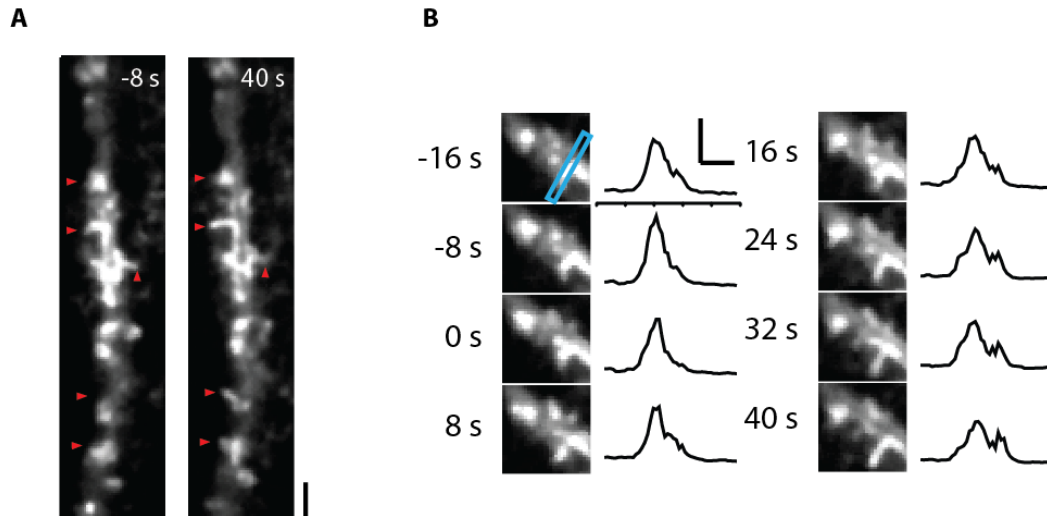


**Figure 21: Local movements of fluorescence into spines. A)** Spine dynamics observed as nanoprobe-labeled receptors move into spine heads. This culture was labeled with nanoprobe and then stimulated with glutamate at time = 0 s. Red arrows point to areas of labeled receptor movement into putative spines. Scale bar is 2.0  $\mu\text{m}$ . **B)** Fluorescence profile of one spine (indicated by blue rectangle) from **(A)** demonstrating the movement of receptors into the spine. Scale bar; x = 1.0  $\mu\text{m}$ , y = 500 AU.

### Tracked movements of nanoprobe-labeled receptors: DIV 1-2

To visualize receptor locations earlier in neuronal development, live cells were treated with nanoprobe within 1 to 2 days of plating. DIV 1–2 neuronal cultures were washed with ECS and incubated with 300 nM nanoprobe for 5 minutes, washed again, and imaged to compile a time-series. In contrast to the punctate labeling patterns found in older cells treated with nanoprobe, in DIV 1-2 cells labeled with nanoprobe we found intricate networks of fluorescent tubular vesicles traveling along neurites, and in and out of the soma (Figure 22, Movies S4 and S5). Additionally, often a concentration of fluorescence appeared to be gathered internally, on one side of the soma. Based on visual comparison the fluorescent tubular networks resembled the TransGolgi

Network (TGN) (Horton et al., 2005), while the tubular vesicles themselves appeared similar to mitochondria (Kramer & Enquist, 2012).

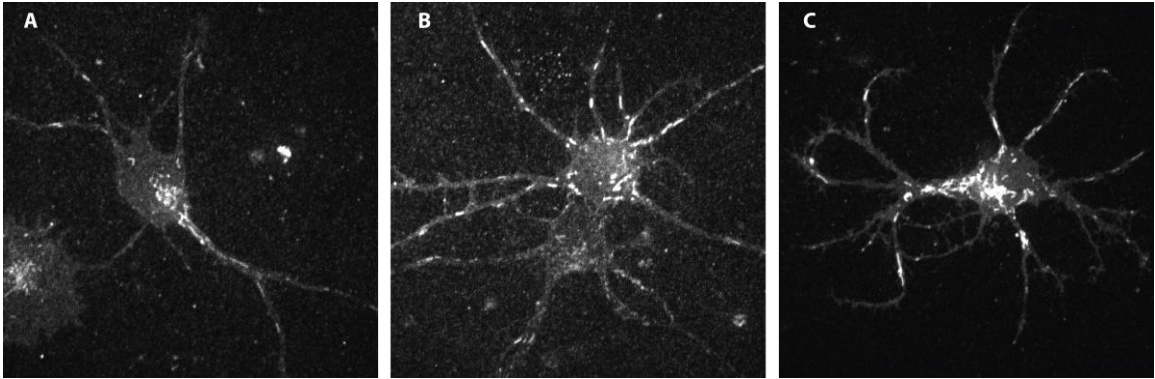


**Figure 22: Dynamic tubular vesicles in DIV 1 dissociated hippocampal neurons treated with nanoprobe.** Neurons were washed with ECS, incubated with 300 nM for 5 minutes, and washed again.

As discussed in the introduction, CP-AMPA receptors are known to be widely expressed in early stages of neuron development. The amount of fluorescent labeling was more widespread than expected, though, leading us to wonder if it could be due to some sort of non-specific interaction, independent of nanoprobe binding to CP-AMPA receptors. However, preliminary experiments with NASPM and DNQX suggested that neuron

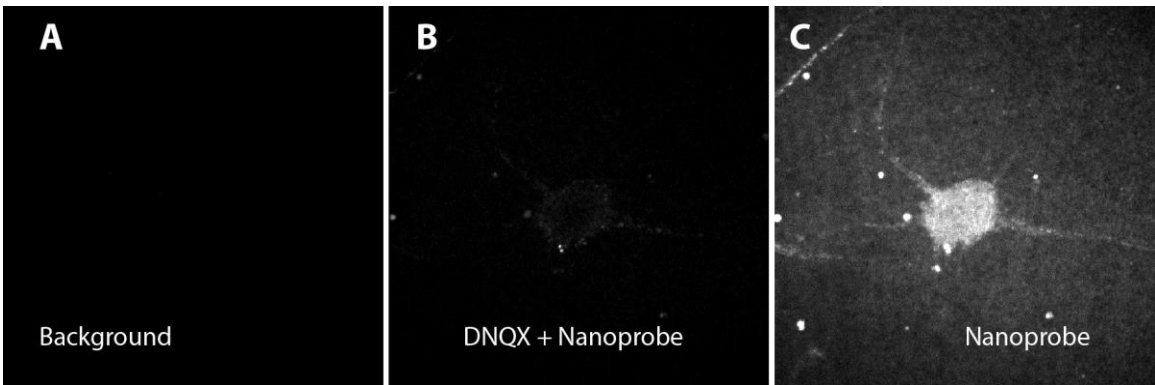


**Figure 23: Competitive antagonist DNQX blocks nanoprobe labeling of DIV 1-2 neurons.** Representative treatment series. DIV 2 neurons washed with ECS and imaged (A), co-treated with 10  $\mu$ M DNQX and 300 nM nanoprobe for 5 minutes, washed and imaged (B), and finally treated with 300 nM nanoprobe alone for 5 minutes, washed and imaged again (C). All brightness and contrast settings are identical.

fluorescence was largely dependent on NASPM-sensitive glutamate receptor activity. When nanoprobe treatment was paired with NASPM or DNQX, fluorescent labeling was greatly reduced compared to follow-up images of the same fields of view after treatment with nanoprobe alone. Representative examples can be seen in Figures 20 and 21.

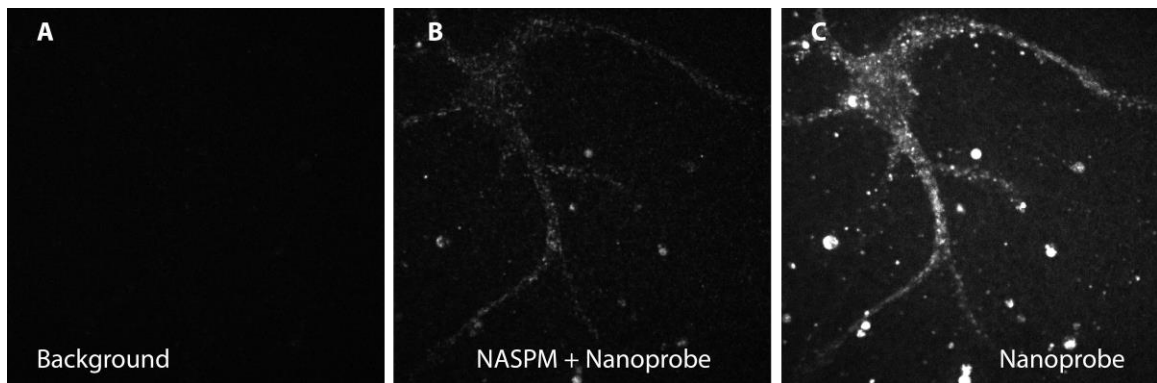


**Figure 24: Competitive antagonist NASPM blocks nanoprobe labeling of DIV 1-2 neurons.** Representative treatment series. DIV 1 neurons washed with ECS and imaged (**A**), co-treated with 300 nM NASPM and 300 nM nanoprobe for 5 minutes, washed and imaged (**B**), and finally treated with 300 nM nanoprobe alone for 5 minutes, washed and imaged again (**C**). All brightness and contrast settings are identical.

Due to the visual similarity between the labeled tubular vesicles and neuronal mitochondria (Stommel et al., 2007) preliminary experiments were conducted in which coverslips of dissociated hippocampal DIV 1-2 neurons were co-treated with both nanoprobe and the mitochondrial label MitoTracker Green FM from Cell Signaling Technology to determine if both fluorophores labeled the same structures. Coverslips were washed 3 times with ECS, incubated with 300 nM nanoprobe for 5 minutes, washed 3 times again, incubated with 500 nM MitoTracker for 1 minute, washed a final time with ECS and imaged. In cells labeled with nanoprobe, nearly every structure labeled with probe appeared to be co-labeled with MitoTracker,

including tubules (Figures 25-27). However, many cells were labeled with MitoTracker that had no nanoprobe labeling whatsoever, reinforcing the idea that though the nanoprobe labeling was abundant in certain DIV 1-2 cells, it was still cell-specific (Figure 26). This specificity, combined with an apparent dependence on active glutamate receptors as suggested by the early DNQX and NASPM experiments supports the possibility that the labeling of young neurons with nanoprobe still depends on CP-AMPA expression.

However, if these are CP-AMPA receptors being expressed and labeled by nanoprobe, they seem to have largely been internalized and possibly packaged with mitochondria or other dynamic tubules to be carried away on normal vesicular routes. It is known that mitochondria linger near synapses where high concentrations of calcium aggregate, in fact cytosolic calcium is a primary regulator of mitochondrial movement. Increased cytosolic calcium due to a variety of sources, including  $\text{Ca}^{2+}$  influx through ionotropic glutamate receptors, halts both anterograde and retrograde mitochondrial movement (Macaskill et al., 2009; Schwarz, 2013). It is believed that mitochondria are regulated in this way so that they can act as calcium buffers in regions of excess calcium, and as a source of ATP for active transport of calcium from the cell. Given this putative role of mitochondria in managing excess calcium, it seems plausible that they would 'linger' near surface-expressed CP-AMPA receptors, which, if active, would presumably be allowing  $\text{Ca}^{2+}$  to influx into the neurons. This does not clarify why these receptors would be internalized and 'packaged' with mitochondria for transport, other than that the mitochondria were located nearby.

It would be interesting to more fully explore the apparent CP-AMPA activity in DIV 1-2 neurons, we certainly weren't expecting them to be trafficked so robustly, apparently along-side mitochondria. Given more time, it would be interesting to attempt to fix and stain DIV 1-2 nanoprobe-treated neurons with antibodies to various endosomal compartments, to track the progress of nanoprobe-labeled receptors. Endocytosis is often conceptualized as a uni-directional pathway starting with the intake of cargo molecules from the plasma membrane, which are then trafficked either to the site where the cargo is needed, or to lysosomes for degradation. However, endocytic trafficking patterns are frequently more complex and can even involve transport directly to and from the TGN, which is typically thought of solely in terms of its role in the secretory pathway. Cargo designated for destruction can be trafficked to lysosomes via late endosomes, while cargo being returned to the surface may be re-inserted directly back into the plasma membrane from the early endosome that initially engulfed it. Cargos designated for insertion/return to other regions of plasma membrane may be carried in recycling endosomes and "tubular intermediates", and as mentioned earlier cargoes may be transported from endosomes to the TGN or directly from the TGN to endosomes without insertion into the plasma membrane first (Yap & Winckler, 2012). Further complicating matters, in polarized cells such as neurons, the TGN plays a role in polarized sorting of cargoes to the somatodendritic membrane or the axonal membrane. Proteins may be directly trafficked to the correct location from the TGN, trafficked via endosomes, or inserted into the non-target membrane domain and then endocytosed and trafficked to the correct domain via a process called transcytosis (Yap & Winckler, 2012). Given this, newly plated cells (DIV 1-2) might have higher rates of endocytosis and sorting as they polarize, though it is

worth keeping in mind that in the standard E18 dissociated rat hippocampal cultures, most plated neurons were polarized prior to dissociation, and they may retain certain aspects of that initial polarization (Polleux & Snider, 2010). This could have an impact on receptor trafficking as well.

Overall, we were surprised to observe the relative abundance of labeling when using nanoprobe on hippocampal neurons during live imaging experiments, particularly given the prior difficulties in identifying probe-labeled receptors on fixed cells. We speculated that this finding could suggest that these cells express more CP-AMPA receptors than previously thought, that there are more NASPM targets that are also sensitive to DNQX block, or both. Our experiments with labeling endogenous glutamate receptors on live dissociated hippocampal neurons with nanoprobe have provided supporting evidence that indeed nanoprobe is targeting NASPM-sensitive glutamate receptors, as demonstrated by the effectiveness of the NASPM and DNQX blocks to probe labeling. CP-AMPA receptors are the most likely candidate, given the specificity of NASPM for CP-AMPA receptors (Koike et al., 1997), particularly at lower concentrations. Furthermore, the trafficking data for older neurons (DIV 14-17) seems to line up well with reported GluA1 and GluA2 trafficking data using genetically engineered receptors (Ju et al., 2004; Washbourne et al., 2002). This suggests that not only might we be able to accurately target a phenotypically-distinct subset of ionotropic glutamate receptors, but we might be able to do this in a way that minimizes disruptions caused by genetic engineering or large antibodies, as was part of our original goal. If we were able to take the next steps of tracking the movement of these nanoprobe-labeled receptors over time, particularly in DIV 1-2 neurons, we could

potentially learn much more about the sorting and transportation of receptor subunits. Perhaps given a sufficient variety of nanoprobe fluorophores, we could visualize different ‘waves’ of receptors internalized, mixed and re-expressed, creating AMPARs colorfully labeled with different fluorophores.

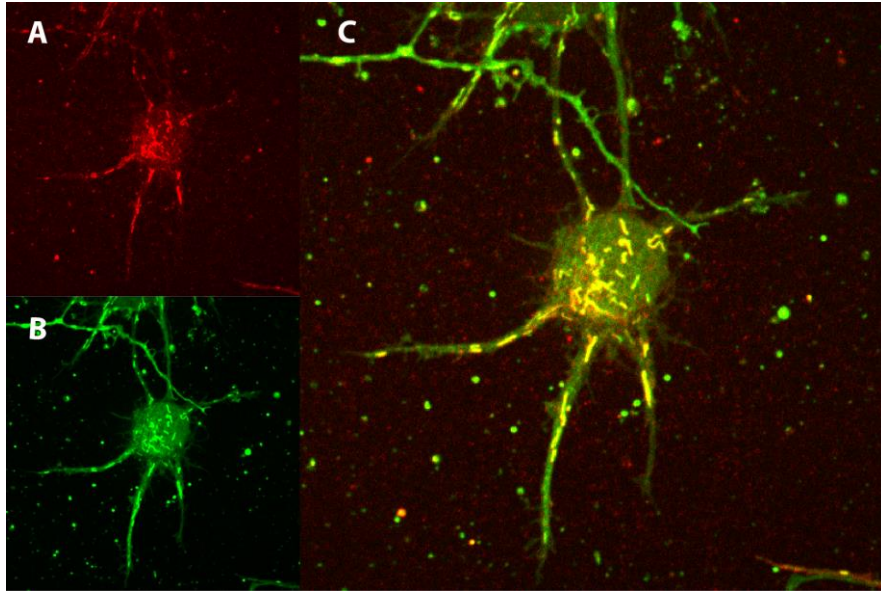


**Figure 25: Dual-labeling of DIV 1 neurons with nanoprobe and a mitochondrial label shows extensive overlap.** DIV 1 dissociated hippocampal cultures were washed 3 times, incubated for 5 minutes with 300 nM nanoprobe (red), washed 3 more times, incubated for 1 minute with the 500 nM of the mitochondrial label MitoTracker Green FM from Cell Signaling Technology (green). **A**) depicts nanoprobe labeling (red), **B**) depicts MitoTracker labeling (green), and **C**) is a composite of the two images. Yellow regions indicate areas of overlap between the labels.

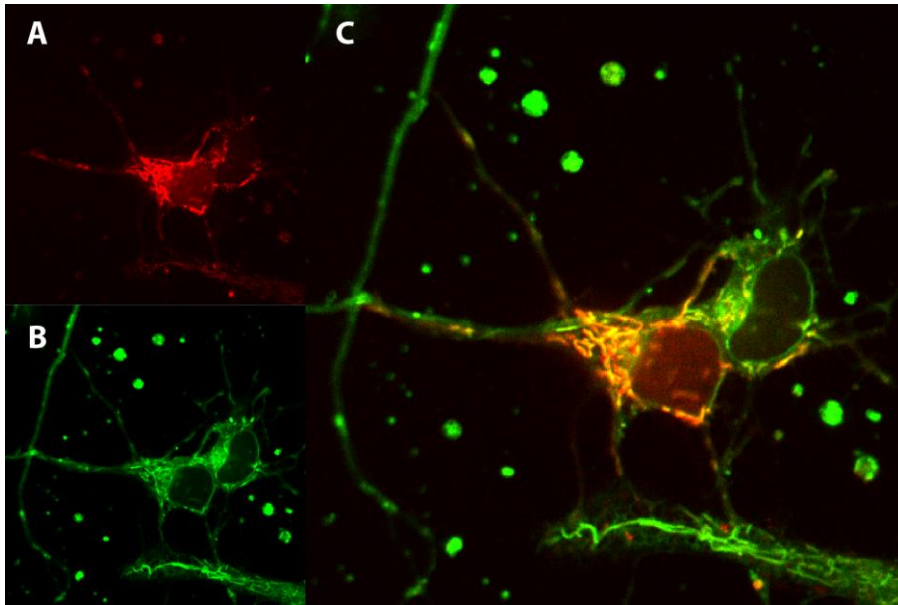
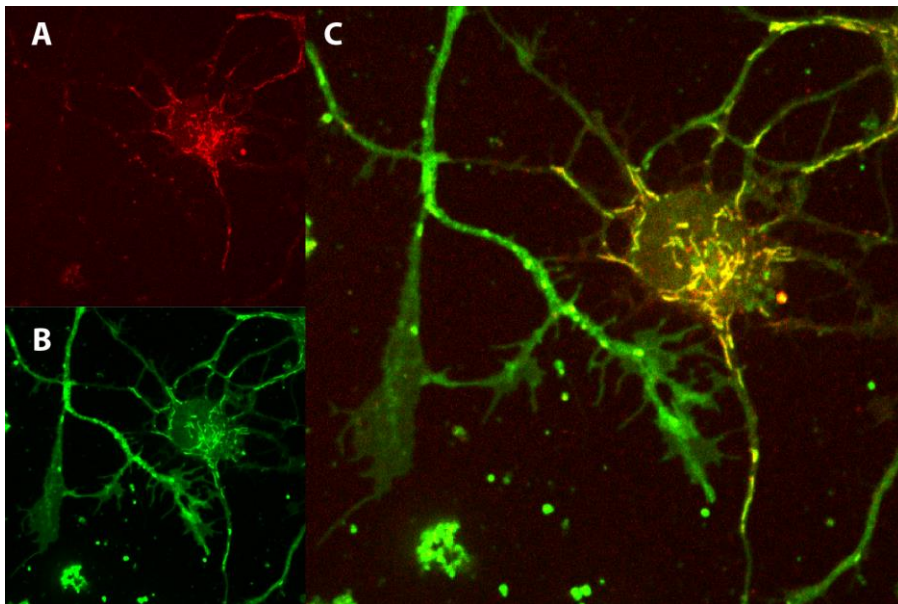


**Figure 26 (above) and 27 (below): Dual-labeling of DIV 1 neurons with nanoprobe and a mitochondrial label shows extensive overlap, and clear delineations where overlap ends.** DIV 1 dissociated hippocampal cultures were washed 3 times, incubated for 5 minutes with 300 nM nanoprobe (red), washed 3 more times, incubated for 1 minute with the 500 nM of the mitochondrial label MitoTracker Green FM from Cell Signaling Technology (green). **A)** depicts nanoprobe labeling (red), **B)** depicts MitoTracker labeling (green), and **C)** is a composite of the two images. Yellow regions indicate areas of overlap between the labels. The extensive overlap of nanoprobe label and mitochondrial label in one cell, with almost no overlap in the neighboring cell, supports the supposition that probe is labeling specific, NASPM-sensitive glutamate-receptors only expressed by certain cells, likely CP-AMPA receptors.



## REFERENCES

- Adesnik, H., & Nicoll, R. A. (2007). Conservation of glutamate receptor 2-containing AMPA receptors during long-term potentiation. *J Neurosci*, *27*(17), 4598-4602. doi: 10.1523/JNEUROSCI.0325-07.2007
- Angulo, M. C., Rossier, J., & Audinat, E. (1999). Postsynaptic glutamate receptors and integrative properties of fast-spiking interneurons in the rat neocortex. *J Neurophysiol*, *82*(3), 1295-1302.
- Argilli, E., Sibley, D. R., Malenka, R. C., England, P. M., & Bonci, A. (2008). Mechanism and time course of cocaine-induced long-term potentiation in the ventral tegmental area. *J Neurosci*, *28*(37), 9092-9100. doi: 10.1523/JNEUROSCI.1001-08.2008
- Bähring, R., & Mayer, M. L. (1998). An analysis of philanthotoxin block for recombinant rat GluR6(Q) glutamate receptor channels. *J Physiol*, *509* ( Pt 3), 635-650.
- Bellone, C., & Luscher, C. (2006). Cocaine triggered AMPA receptor redistribution is reversed in vivo by mGluR-dependent long-term depression. *Nat Neurosci*, *9*(5), 636-641. doi: 10.1038/nn1682
- Beppu, K., Sasaki, T., Tanaka, K. F., Yamanaka, A., Fukazawa, Y., Shigemoto, R., & Matsui, K. (2014). Optogenetic countering of glial acidosis suppresses glial glutamate release and ischemic brain damage. *Neuron*, *81*(2), 314-320. doi: 10.1016/j.neuron.2013.11.011
- Blaschke, M., Keller, B. U., Rivosecchi, R., Hollmann, M., Heinemann, S., & Konnerth, A. (1993). A single amino acid determines the subunit-specific spider toxin block of alpha-amino-3-hydroxy-5-methylisoxazole-4-propionate/kainate receptor channels. *Proc Natl Acad Sci U S A*, *90*(14), 6528-6532.
- Bliss, T. V., & Collingridge, G. L. (1993). A synaptic model of memory: long-term potentiation in the hippocampus. *Nature*, *361*(6407), 31-39. doi: 10.1038/361031a0
- Borgland, S. L., Malenka, R. C., & Bonci, A. (2004). Acute and chronic cocaine-induced potentiation of synaptic strength in the ventral tegmental area: electrophysiological and behavioral correlates in individual rats. *J Neurosci*, *24*(34), 7482-7490. doi: 10.1523/JNEUROSCI.1312-04.2004
- Bourne, J. N., & Harris, K. M. (2008). Balancing structure and function at hippocampal dendritic spines. *Annu Rev Neurosci*, *31*, 47-67. doi: 10.1146/annurev.neuro.31.060407.125646

- Bowie, D., & Mayer, M. L. (1995). Inward rectification of both AMPA and kainate subtype glutamate receptors generated by polyamine-mediated ion channel block. *Neuron*, *15*(2), 453-462.
- Brackley, P. T., Bell, D. R., Choi, S. K., Nakanishi, K., & Usherwood, P. N. (1993). Selective antagonism of native and cloned kainate and NMDA receptors by polyamine-containing toxins. *J Pharmacol Exp Ther*, *266*(3), 1573-1580.
- Brill, J., & Huguenard, J. R. (2008). Sequential changes in AMPA receptor targeting in the developing neocortical excitatory circuit. *J Neurosci*, *28*(51), 13918-13928. doi: 10.1523/JNEUROSCI.3229-08.2008
- Camire, O., & Topolnik, L. (2014). Dendritic calcium nonlinearities switch the direction of synaptic plasticity in fast-spiking interneurons. *J Neurosci*, *34*(11), 3864-3877. doi: 10.1523/JNEUROSCI.2253-13.2014
- Carroll, R. C., Beattie, E. C., von Zastrow, M., & Malenka, R. C. (2001). Role of AMPA receptor endocytosis in synaptic plasticity. *Nat Rev Neurosci*, *2*(5), 315-324. doi: 10.1038/35072500
- Chater, T. E., & Goda, Y. (2014). The role of AMPA receptors in postsynaptic mechanisms of synaptic plasticity. *Front Cell Neurosci*, *8*, 401. doi: 10.3389/fncel.2014.00401
- Chen, B. T., Bowers, M. S., Martin, M., Hopf, F. W., Guillory, A. M., Carelli, R. M., . . . Bonci, A. (2008). Cocaine but not natural reward self-administration nor passive cocaine infusion produces persistent LTP in the VTA. *Neuron*, *59*(2), 288-297. doi: 10.1016/j.neuron.2008.05.024
- Clem, R. L., & Huganir, R. L. (2010). Calcium-permeable AMPA receptor dynamics mediate fear memory erasure. *Science*, *330*(6007), 1108-1112. doi: 10.1126/science.1195298
- Conrad, K. L., Tseng, K. Y., Uejima, J. L., Reimers, J. M., Heng, L. J., Shaham, Y., . . . Wolf, M. E. (2008). Formation of accumbens GluR2-lacking AMPA receptors mediates incubation of cocaine craving. *Nature*, *454*(7200), 118-121. doi: 10.1038/nature06995
- Cull-Candy, S., Kelly, L., & Farrant, M. (2006). Regulation of Ca<sup>2+</sup>-permeable AMPA receptors: synaptic plasticity and beyond. *Curr Opin Neurobiol*, *16*(3), 288-297. doi: 10.1016/j.conb.2006.05.012
- Davalos, A., Shuaib, A., & Wahlgren, N. G. (2000). Neurotransmitters and pathophysiology of stroke: evidence for the release of glutamate and other transmitters/mediators in animals and humans. *J Stroke Cerebrovasc Dis*, *9*(6 Pt 2), 2-8. doi: 10.1053/jscd.2000.18908

- Dong, H., & Zhou, H. X. (2011). Atomistic mechanism for the activation and desensitization of an AMPA-subtype glutamate receptor. *Nat Commun*, 2, 354. doi: 10.1038/ncomms1362
- Eybalin, M., Caicedo, A., Renard, N., Ruel, J., & Puel, J. L. (2004). Transient Ca<sup>2+</sup>-permeable AMPA receptors in postnatal rat primary auditory neurons. *Eur J Neurosci*, 20(11), 2981-2989. doi: 10.1111/j.1460-9568.2004.03772.x
- Goldberg, J. H., Tamas, G., Aronov, D., & Yuste, R. (2003). Calcium microdomains in aspiny dendrites. *Neuron*, 40(4), 807-821.
- Gong, L. Q., He, L. J., Dong, Z. Y., Lu, X. H., Poo, M. M., & Zhang, X. H. (2011). Postinduction requirement of NMDA receptor activation for late-phase long-term potentiation of developing retinotectal synapses in vivo. *J Neurosci*, 31(9), 3328-3335. doi: 10.1523/JNEUROSCI.5936-10.2011
- Gouaux, E. (2004). Structure and function of AMPA receptors. *J Physiol*, 554(Pt 2), 249-253. doi: 10.1113/jphysiol.2003.054320
- Griguoli, M., Cellot, G., & Cherubini, E. (2013). In hippocampal oriens interneurons anti-Hebbian long-term potentiation requires cholinergic signaling via alpha7 nicotinic acetylcholine receptors. *J Neurosci*, 33(3), 1044-1049. doi: 10.1523/JNEUROSCI.1070-12.2013
- Gruber, H. J., Hahn, C. D., Kada, G., Riener, C. K., Harms, G. S., Ahrer, W., . . . Knaus, H. G. (2000). Anomalous fluorescence enhancement of Cy3 and cy3.5 versus anomalous fluorescence loss of Cy5 and Cy7 upon covalent linking to IgG and noncovalent binding to avidin. *Bioconjug Chem*, 11(5), 696-704.
- Hainmuller, T., Krieglstein, K., Kulik, A., & Bartos, M. (2014). Joint CP-AMPA and group I mGlu receptor activation is required for synaptic plasticity in dentate gyrus fast-spiking interneurons. *Proc Natl Acad Sci U S A*, 111(36), 13211-13216. doi: 10.1073/pnas.1409394111
- Hideyama, T., Yamashita, T., Aizawa, H., Tsuji, S., Kakita, A., Takahashi, H., & Kwak, S. (2012). Profound downregulation of the RNA editing enzyme ADAR2 in ALS spinal motor neurons. *Neurobiol Dis*, 45(3), 1121-1128. doi: 10.1016/j.nbd.2011.12.033
- Hideyama, T., Yamashita, T., Suzuki, T., Tsuji, S., Higuchi, M., Seeburg, P. H., . . . Kwak, S. (2010). Induced loss of ADAR2 engenders slow death of motor neurons from Q/R site-unedited GluR2. *J Neurosci*, 30(36), 11917-11925. doi: 10.1523/JNEUROSCI.2021-10.2010

- Ho, M. T., Pelkey, K. A., Topolnik, L., Petralia, R. S., Takamiya, K., Xia, J., . . . McBain, C. J. (2007). Developmental expression of Ca<sup>2+</sup>-permeable AMPA receptors underlies depolarization-induced long-term depression at mossy fiber CA3 pyramid synapses. *J Neurosci*, *27*(43), 11651-11662. doi: 10.1523/JNEUROSCI.2671-07.2007
- Holmes-Farley, S. R., & Whitesides, G. M. (1985). Fluorescence Properties of Dansyl Groups Covalently Bonded to the Surface of Oxidatively Functionalized Low-Density Polyethylene Film. *Langmuir*, *2*(3), 266-282.
- Horton, A. C., Racz, B., Monson, E. E., Lin, A. L., Weinberg, R. J., & Ehlers, M. D. (2005). Polarized secretory trafficking directs cargo for asymmetric dendrite growth and morphogenesis. *Neuron*, *48*(5), 757-771. doi: 10.1016/j.neuron.2005.11.005
- Huganir, R. L., & Nicoll, R. A. (2013). AMPARs and synaptic plasticity: the last 25 years. *Neuron*, *80*(3), 704-717. doi: 10.1016/j.neuron.2013.10.025
- Iino, M., Koike, M., Isa, T., & Ozawa, S. (1996). Voltage-dependent blockage of Ca(2+)-permeable AMPA receptors by joro spider toxin in cultured rat hippocampal neurones. *J Physiol*, *496* ( Pt 2), 431-437.
- Jackson, A. C., Milstein, A. D., Soto, D., Farrant, M., Cull-Candy, S. G., & Nicoll, R. A. (2011). Probing TARP modulation of AMPA receptor conductance with polyamine toxins. *J Neurosci*, *31*(20), 7511-7520. doi: 10.1523/JNEUROSCI.6688-10.2011
- Janeway, C. A., Jr. , Travers, P., Walport, M., & Shlomchik, M. J. (2001). The interaction of the antibody molecule with specific antigen *Immunobiology: The Immune System in Health and Disease*. (5th ed.). New York: Garland Science.
- Ju, W., Morishita, W., Tsui, J., Gaietta, G., Deerinck, T. J., Adams, S. R., . . . Malenka, R. C. (2004). Activity-dependent regulation of dendritic synthesis and trafficking of AMPA receptors. *Nat Neurosci*, *7*(3), 244-253. doi: 10.1038/nn1189
- Kawahara, Y., Ito, K., Sun, H., Aizawa, H., Kanazawa, I., & Kwak, S. (2004). Glutamate receptors: RNA editing and death of motor neurons. *Nature*, *427*(6977), 801. doi: 10.1038/427801a
- Kawahara, Y., Kwak, S., Sun, H., Ito, K., Hashida, H., Aizawa, H., . . . Kanazawa, I. (2003). Human spinal motoneurons express low relative abundance of GluR2 mRNA: an implication for excitotoxicity in ALS. *J Neurochem*, *85*(3), 680-689.
- Kessels, H. W., & Malinow, R. (2009). Synaptic AMPA receptor plasticity and behavior. *Neuron*, *61*(3), 340-350. doi: 10.1016/j.neuron.2009.01.015

- Kiernan, M. C., Vucic, S., Cheah, B. C., Turner, M. R., Eisen, A., Hardiman, O., . . . Zoing, M. C. (2011). Amyotrophic lateral sclerosis. *Lancet*, *377*(9769), 942-955. doi: 10.1016/S0140-6736(10)61156-7
- Koike, M., Iino, M., & Ozawa, S. (1997). Blocking effect of 1-naphthyl acetyl spermine on Ca(2+)-permeable AMPA receptors in cultured rat hippocampal neurons. *Neurosci Res*, *29*(1), 27-36.
- Kramer, T., & Enquist, L. W. (2012). Alpha herpesvirus infection disrupts mitochondrial transport in neurons. *Cell Host Microbe*, *11*(5), 504-514. doi: 10.1016/j.chom.2012.03.005
- Kullmann, D. M., & Lamsa, K. (2008). Roles of distinct glutamate receptors in induction of anti-Hebbian long-term potentiation. *J Physiol*, *586*(6), 1481-1486. doi: 10.1113/jphysiol.2007.148064
- Kullmann, D. M., & Lamsa, K. P. (2007). Long-term synaptic plasticity in hippocampal interneurons. *Nat Rev Neurosci*, *8*(9), 687-699. doi: 10.1038/nrn2207
- Kumar, S. S., Bacci, A., Kharazia, V., & Huguenard, J. R. (2002). A developmental switch of AMPA receptor subunits in neocortical pyramidal neurons. *J Neurosci*, *22*(8), 3005-3015. doi: 20026285
- Kwak, S., & Weiss, J. H. (2006). Calcium-permeable AMPA channels in neurodegenerative disease and ischemia. *Curr Opin Neurobiol*, *16*(3), 281-287. doi: 10.1016/j.conb.2006.05.004
- Laezza, F., & Dingledine, R. (2011). Induction and expression rules of synaptic plasticity in hippocampal interneurons. *Neuropharmacology*, *60*(5), 720-729. doi: 10.1016/j.neuropharm.2010.12.016
- Lamsa, K. P., Heeroma, J. H., Somogyi, P., Rusakov, D. A., & Kullmann, D. M. (2007). Anti-Hebbian long-term potentiation in the hippocampal feedback inhibitory circuit. *Science*, *315*(5816), 1262-1266. doi: 10.1126/science.1137450
- Lau, A., & Tymianski, M. (2010). Glutamate receptors, neurotoxicity and neurodegeneration. *Pflugers Arch*, *460*(2), 525-542. doi: 10.1007/s00424-010-0809-1
- Le Duigou, C., & Kullmann, D. M. (2011). Group I mGluR agonist-evoked long-term potentiation in hippocampal oriens interneurons. *J Neurosci*, *31*(15), 5777-5781. doi: 10.1523/JNEUROSCI.6265-10.2011

- Le Roux, N., Cabezas, C., Bohm, U. L., & Poncer, J. C. (2013). Input-specific learning rules at excitatory synapses onto hippocampal parvalbumin-expressing interneurons. *J Physiol*, *591*(Pt 7), 1809-1822. doi: 10.1113/jphysiol.2012.245852
- Li, J., Doyle, K. M., & Tatlisumak, T. (2007). Polyamines in the brain: distribution, biological interactions, and their potential therapeutic role in brain ischaemia. *Curr Med Chem*, *14*(17), 1807-1813.
- Lissin, D. V., Carroll, R. C., Nicoll, R. A., Malenka, R. C., & von Zastrow, M. (1999). Rapid, activation-induced redistribution of ionotropic glutamate receptors in cultured hippocampal neurons. *J Neurosci*, *19*(4), 1263-1272.
- Liu, S. J., & Zukin, R. S. (2007). Ca<sup>2+</sup>-permeable AMPA receptors in synaptic plasticity and neuronal death. *Trends Neurosci*, *30*(3), 126-134. doi: 10.1016/j.tins.2007.01.006
- Loweth, J. A., Scheyer, A. F., Milovanovic, M., LaCrosse, A. L., Flores-Barrera, E., Werner, C. T., . . . Wolf, M. E. (2014). Synaptic depression via mGluR1 positive allosteric modulation suppresses cue-induced cocaine craving. *Nat Neurosci*, *17*(1), 73-80. doi: 10.1038/nn.3590
- Lu, W., Shi, Y., Jackson, A. C., Bjorgan, K., During, M. J., Sprengel, R., . . . Nicoll, R. A. (2009). Subunit composition of synaptic AMPA receptors revealed by a single-cell genetic approach. *Neuron*, *62*(2), 254-268. doi: 10.1016/j.neuron.2009.02.027
- Luscher, C., & Malenka, R. C. (2012). NMDA receptor-dependent long-term potentiation and long-term depression (LTP/LTD). *Cold Spring Harb Perspect Biol*, *4*(6). doi: 10.1101/cshperspect.a005710
- Macaskill, A. F., Rinholm, J. E., Twelvetrees, A. E., Arancibia-Carcamo, I. L., Muir, J., Fransson, A., . . . Kittler, J. T. (2009). Miro1 is a calcium sensor for glutamate receptor-dependent localization of mitochondria at synapses. *Neuron*, *61*(4), 541-555. doi: 10.1016/j.neuron.2009.01.030
- Malenka, R. C., & Bear, M. F. (2004). LTP and LTD: an embarrassment of riches. *Neuron*, *44*(1), 5-21. doi: 10.1016/j.neuron.2004.09.012
- Mameli, M., Balland, B., Lujan, R., & Luscher, C. (2007). Rapid synthesis and synaptic insertion of GluR2 for mGluR-LTD in the ventral tegmental area. *Science*, *317*(5837), 530-533. doi: 10.1126/science.1142365
- Mameli, M., Halbout, B., Creton, C., Engblom, D., Parkitna, J. R., Spanagel, R., & Luscher, C. (2009). Cocaine-evoked synaptic plasticity: persistence in the VTA triggers adaptations in the NAc. *Nat Neurosci*, *12*(8), 1036-1041. doi: 10.1038/nn.2367

- Mangiavacchi, S., & Wolf, M. E. (2004). D1 dopamine receptor stimulation increases the rate of AMPA receptor insertion onto the surface of cultured nucleus accumbens neurons through a pathway dependent on protein kinase A. *J Neurochem*, *88*(5), 1261-1271.
- Mattison, H. A., Bagal, A. A., Mohammadi, M., Pulimood, N. S., Reich, C. G., Alger, B. E., . . . Thompson, S. M. (2014). Evidence of calcium-permeable AMPA receptors in dendritic spines of CA1 pyramidal neurons. *J Neurophysiol*, *112*(2), 263-275. doi: 10.1152/jn.00578.2013
- McCutcheon, J. E., Wang, X., Tseng, K. Y., Wolf, M. E., & Marinelli, M. (2011). Calcium-permeable AMPA receptors are present in nucleus accumbens synapses after prolonged withdrawal from cocaine self-administration but not experimenter-administered cocaine. *J Neurosci*, *31*(15), 5737-5743. doi: 10.1523/JNEUROSCI.0350-11.2011
- Mellor, I. R., Brier, T. J., Pluteanu, F., Stromgaard, K., Saghyan, A., Eldursi, N., . . . Usherwood, P. N. (2003). Modification of the philanthotoxin-343 polyamine moiety results in different structure-activity profiles at muscle nicotinic ACh, NMDA and AMPA receptors. *Neuropharmacology*, *44*(1), 70-80.
- Migues, P. V., Cammarota, M., Kavanagh, J., Atkinson, R., Powis, D. A., & Rostas, J. A. (2007). Maturation changes in the subunit composition of AMPA receptors and the functional consequences of their activation in chicken forebrain. *Dev Neurosci*, *29*(3), 232-240. doi: 10.1159/000096408
- Mitchell, N. A., & Fleck, M. W. (2007). Targeting AMPA receptor gating processes with allosteric modulators and mutations. *Biophys J*, *92*(7), 2392-2402. doi: 10.1529/biophysj.106.095091
- Monici, M. (2005). Cell and tissue autofluorescence research and diagnostic applications. *Biotechnol Annu Rev*, *11*, 227-256. doi: 10.1016/S1387-2656(05)11007-2
- Mony, L., Kew, J. N., Gunthorpe, M. J., & Paoletti, P. (2009). Allosteric modulators of NR2B-containing NMDA receptors: molecular mechanisms and therapeutic potential. *Br J Pharmacol*, *157*(8), 1301-1317. doi: 10.1111/j.1476-5381.2009.00304.x
- Mott, D. D., Washburn, M. S., Zhang, S., & Dingledine, R. J. (2003). Subunit-dependent modulation of kainate receptors by extracellular protons and polyamines. *J Neurosci*, *23*(4), 1179-1188.
- Nagarajan, N., Quast, C., Boxall, A. R., Shahid, M., & Rosenmund, C. (2001). Mechanism and impact of allosteric AMPA receptor modulation by the ampakine CX546. *Neuropharmacology*, *41*(6), 650-663.

- Nicholson, E., & Kullmann, D. M. (2014). Long-term potentiation in hippocampal oriens interneurons: postsynaptic induction, presynaptic expression and evaluation of candidate retrograde factors. *Philos Trans R Soc Lond B Biol Sci*, 369(1633), 20130133. doi: 10.1098/rstb.2013.0133
- Nissen, W., Szabo, A., Somogyi, J., Somogyi, P., & Lamsa, K. P. (2010). Cell type-specific long-term plasticity at glutamatergic synapses onto hippocampal interneurons expressing either parvalbumin or CB1 cannabinoid receptor. *J Neurosci*, 30(4), 1337-1347. doi: 10.1523/JNEUROSCI.3481-09.2010
- Noh, K. M., Yokota, H., Mashiko, T., Castillo, P. E., Zukin, R. S., & Bennett, M. V. (2005). Blockade of calcium-permeable AMPA receptors protects hippocampal neurons against global ischemia-induced death. *Proc Natl Acad Sci U S A*, 102(34), 12230-12235. doi: 10.1073/pnas.0505408102
- Ogoshi, F., & Weiss, J. H. (2003). Heterogeneity of Ca<sup>2+</sup>-permeable AMPA/kainate channel expression in hippocampal pyramidal neurons: fluorescence imaging and immunocytochemical assessment. *J Neurosci*, 23(33), 10521-10530.
- Oren, I., Nissen, W., Kullmann, D. M., Somogyi, P., & Lamsa, K. P. (2009). Role of ionotropic glutamate receptors in long-term potentiation in rat hippocampal CA1 oriens-lacunosum moleculare interneurons. *J Neurosci*, 29(4), 939-950. doi: 10.1523/JNEUROSCI.3251-08.2009
- Orrenius, S., Zhivotovsky, B., & Nicotera, P. (2003). Regulation of cell death: the calcium-apoptosis link. *Nat Rev Mol Cell Biol*, 4(7), 552-565. doi: 10.1038/nrm1150
- Patten, S. A., & Ali, D. W. (2007). AMPA receptors associated with zebrafish Mauthner cells switch subunits during development. *J Physiol*, 581(Pt 3), 1043-1056. doi: 10.1113/jphysiol.2007.129999
- Pelletier, V., Gal, N., Fournier, P., & Kilfoil, M. L. (2009). Microrheology of microtubule solutions and actin-microtubule composite networks. *Phys Rev Lett*, 102(18), 188303. doi: 10.1103/PhysRevLett.102.188303
- Pickens, C. L., Airavaara, M., Theberge, F., Fanous, S., Hope, B. T., & Shaham, Y. (2011). Neurobiology of the incubation of drug craving. *Trends Neurosci*, 34(8), 411-420. doi: 10.1016/j.tins.2011.06.001
- Plant, K., Pelkey, K. A., Bortolotto, Z. A., Morita, D., Terashima, A., McBain, C. J., . . . Isaac, J. T. (2006). Transient incorporation of native GluR2-lacking AMPA receptors during hippocampal long-term potentiation. *Nat Neurosci*, 9(5), 602-604. doi: 10.1038/nn1678

- Polepalli, J. S., Sullivan, R. K., Yanagawa, Y., & Sah, P. (2010). A specific class of interneuron mediates inhibitory plasticity in the lateral amygdala. *J Neurosci*, *30*(44), 14619-14629. doi: 10.1523/JNEUROSCI.3252-10.2010
- Polleux, F., & Snider, W. (2010). Initiating and growing an axon. *Cold Spring Harb Perspect Biol*, *2*(4), a001925. doi: 10.1101/cshperspect.a001925
- Prince, H. C., Tzingounis, A. V., Levey, A. I., & Conn, P. J. (2000). Functional downregulation of GluR2 in piriform cortex of kindled animals. *Synapse*, *38*(4), 489-498. doi: 10.1002/1098-2396(20001215)38:4<489::AID-SYN15>3.0.CO;2-N
- Prince, H. K., Conn, P. J., Blackstone, C. D., Huganir, R. L., & Levey, A. I. (1995). Down-regulation of AMPA receptor subunit GluR2 in amygdaloid kindling. *J Neurochem*, *64*(1), 462-465.
- Saal, D., Dong, Y., Bonci, A., & Malenka, R. C. (2003). Drugs of abuse and stress trigger a common synaptic adaptation in dopamine neurons. *Neuron*, *37*(4), 577-582.
- Sambandan, S., Sauer, J. F., Vida, I., & Bartos, M. (2010). Associative plasticity at excitatory synapses facilitates recruitment of fast-spiking interneurons in the dentate gyrus. *J Neurosci*, *30*(35), 11826-11837. doi: 10.1523/JNEUROSCI.2012-10.2010
- Schmidt, C., & Hollmann, M. (2008). Apparent homomeric NR1 currents observed in *Xenopus* oocytes are caused by an endogenous NR2 subunit. *J Mol Biol*, *376*(3), 658-670. doi: 10.1016/j.jmb.2007.11.105
- Schmidt, C., Klein, C., & Hollmann, M. (2009). *Xenopus laevis* oocytes endogenously express all subunits of the ionotropic glutamate receptor family. *J Mol Biol*, *390*(2), 182-195. doi: 10.1016/j.jmb.2009.05.008
- Schneider, C. A., Rasband, W. S., & Eliceiri, K. W. (2012). NIH Image to ImageJ: 25 years of image analysis. *Nat Methods*, *9*(7), 671-675.
- Schwarz, T. L. (2013). Mitochondrial trafficking in neurons. *Cold Spring Harb Perspect Biol*, *5*(6). doi: 10.1101/cshperspect.a011304
- Sensi, S. L., Paoletti, P., Bush, A. I., & Sekler, I. (2009). Zinc in the physiology and pathology of the CNS. *Nat Rev Neurosci*, *10*(11), 780-791. doi: 10.1038/nrn2734
- Shaw, P. J. (2005). Molecular and cellular pathways of neurodegeneration in motor neurone disease. *J Neurol Neurosurg Psychiatry*, *76*(8), 1046-1057. doi: 10.1136/jnnp.2004.048652

- Sobolevsky, A. I., Rosconi, M. P., & Gouaux, E. (2009). X-ray structure, symmetry and mechanism of an AMPA-subtype glutamate receptor. *Nature*, *462*(7274), 745-756. doi: 10.1038/nature08624
- Soler-Llavina, G. J., & Sabatini, B. L. (2006). Synapse-specific plasticity and compartmentalized signaling in cerebellar stellate cells. *Nat Neurosci*, *9*(6), 798-806. doi: 10.1038/nn1698
- Soloviev, M. M., & Barnard, E. A. (1997). Xenopus oocytes express a unitary glutamate receptor endogenously. *J Mol Biol*, *273*(1), 14-18. doi: 10.1006/jmbi.1997.1272
- Stommel, E. W., van Hoff, R. M., Graber, D. J., Bercury, K. K., Langford, G. M., & Harris, B. T. (2007). Tumor necrosis factor-alpha induces changes in mitochondrial cellular distribution in motor neurons. *Neuroscience*, *146*(3), 1013-1019. doi: 10.1016/j.neuroscience.2007.02.036
- Stromgaard, K., Brierley, M. J., Andersen, K., Slok, F. A., Mellor, I. R., Usherwood, P. N., . . . Jaroszewski, J. W. (1999). Analogues of neuroactive polyamine wasp toxins that lack inner basic sites exhibit enhanced antagonism toward a muscle-type mammalian nicotinic acetylcholine receptor. *J Med Chem*, *42*(25), 5224-5234.
- Stromgaard, K., & Mellor, I. (2004). AMPA receptor ligands: synthetic and pharmacological studies of polyamines and polyamine toxins. *Med Res Rev*, *24*(5), 589-620. doi: 10.1002/med.20004
- Studniarczyk, D., Coombs, I., Cull-Candy, S. G., & Farrant, M. (2013). TARP gamma-7 selectively enhances synaptic expression of calcium-permeable AMPARs. *Nat Neurosci*, *16*(9), 1266-1274. doi: 10.1038/nn.3473
- Sun, H. Y., Bartley, A. F., & Dobrunz, L. E. (2009). Calcium-permeable presynaptic kainate receptors involved in excitatory short-term facilitation onto somatostatin interneurons during natural stimulus patterns. *J Neurophysiol*, *101*(2), 1043-1055. doi: 10.1152/jn.90286.2008
- Szabo, A., Somogyi, J., Cauli, B., Lambolez, B., Somogyi, P., & Lamsa, K. P. (2012). Calcium-permeable AMPA receptors provide a common mechanism for LTP in glutamatergic synapses of distinct hippocampal interneuron types. *J Neurosci*, *32*(19), 6511-6516. doi: 10.1523/JNEUROSCI.0206-12.2012
- Szydlowska, K., & Tymianski, M. (2010). Calcium, ischemia and excitotoxicity. *Cell Calcium*, *47*(2), 122-129. doi: 10.1016/j.ceca.2010.01.003

- Traynelis, S. F., Wollmuth, L. P., McBain, C. J., Menniti, F. S., Vance, K. M., Ogden, K. K., . . . Dingledine, R. (2010). Glutamate receptor ion channels: structure, regulation, and function. *Pharmacol Rev*, 62(3), 405-496. doi: 10.1124/pr.109.002451
- Turina, D., Bjornstrom, K., Sundqvist, T., & Eintrei, C. (2011). Propofol alters vesicular transport in rat cortical neuronal cultures. *J Physiol Pharmacol*, 62(1), 119-124.
- Vandenberghe, W., Robberecht, W., & Brorson, J. R. (2000). AMPA receptor calcium permeability, GluR2 expression, and selective motoneuron vulnerability. *J Neurosci*, 20(1), 123-132.
- Vytla, D., Combs-Bachmann, R. E., Hussey, A. M., Hafez, I., & Chambers, J. J. (2011). Silent, fluorescent labeling of native neuronal receptors. *Org Biomol Chem*, 9(20), 7151-7161. doi: 10.1039/c1ob05963g
- Washbourne, P., Bennett, J. E., & McAllister, A. K. (2002). Rapid recruitment of NMDA receptor transport packets to nascent synapses. *Nat Neurosci*, 5(8), 751-759. doi: 10.1038/nn883
- Washburn, M. S., & Dingledine, R. (1996). Block of alpha-amino-3-hydroxy-5-methyl-4-isoxazolepropionic acid (AMPA) receptors by polyamines and polyamine toxins. *J Pharmacol Exp Ther*, 278(2), 669-678.
- Weilinger, N. L., Maslieieva, V., Bialecki, J., Sridharan, S. S., Tang, P. L., & Thompson, R. J. (2013). Iontropic receptors and ion channels in ischemic neuronal death and dysfunction. *Acta Pharmacol Sin*, 34(1), 39-48. doi: 10.1038/aps.2012.95
- White, S. L., Ortinski, P. I., Friedman, S. H., Zhang, L., Neve, R. L., Kalb, R. G., . . . Pierce, R. C. (2015). A Critical Role for the GluA1 Accessory Protein, SAP97, in Cocaine Seeking. *Neuropsychopharmacology*. doi: 10.1038/npp.2015.199
- Wolf, M. E., & Tseng, K. Y. (2012). Calcium-permeable AMPA receptors in the VTA and nucleus accumbens after cocaine exposure: when, how, and why? *Front Mol Neurosci*, 5, 72. doi: 10.3389/fnmol.2012.00072
- Yamashita, T., & Kwak, S. (2014). The molecular link between inefficient GluA2 Q/R site-RNA editing and TDP-43 pathology in motor neurons of sporadic amyotrophic lateral sclerosis patients. *Brain Res*, 1584, 28-38. doi: 10.1016/j.brainres.2013.12.011
- Yap, C. C., & Winckler, B. (2012). Harnessing the power of the endosome to regulate neural development. *Neuron*, 74(3), 440-451. doi: 10.1016/j.neuron.2012.04.015

- Yin, H. Z., Sensi, S. L., Ogoshi, F., & Weiss, J. H. (2002). Blockade of Ca<sup>2+</sup>-permeable AMPA/kainate channels decreases oxygen-glucose deprivation-induced Zn<sup>2+</sup> accumulation and neuronal loss in hippocampal pyramidal neurons. *J Neurosci*, 22(4), 1273-1279.
- Yoneda, Y., Kawajiri, S., Hasegawa, A., Kito, F., Katano, S., Takano, E., & Mimura, T. (2001). Synthesis of polyamine derivatives having non-hypotensive Ca<sup>2+</sup>-permeable AMPA receptor antagonist activity. *Bioorg Med Chem Lett*, 11(10), 1261-1264.
- Yuste, R., & Denk, W. (1995). Dendritic spines as basic functional units of neuronal integration. *Nature*, 375(6533), 682-684. doi: 10.1038/375682a0
- Zack, G. W., Rogers, W. E., & Latt, S. A. (1977). Automatic measurement of sister chromatid exchange frequency. *J Histochem Cytochem*, 25(7), 741-753.
- Zinman, L., & Cudkovicz, M. (2011). Emerging targets and treatments in amyotrophic lateral sclerosis. *Lancet Neurol*, 10(5), 481-490. doi: 10.1016/S1474-4422(11)70024-2